Journal of Pharmaceutical Sciences 110 (2021) 1349-1364

Contents lists available at ScienceDirect

Journal of Pharmaceutical Sciences

journal homepage: www.jpharmsci.org

Pharmaceutical Nanotechnology

The Inclusion of a Matrix Metalloproteinase-9 Responsive Sequence in Self-assembled Peptide-based Brain-Targeting Nanoparticles Improves the Efficiency of Nanoparticles Crossing the Blood-Brain Barrier at Elevated MMP-9 Levels

Yamir Islam [a], Parinaz Ehtezazi [a], Andrew Cashmore [a], Elena Marinsalda [a], Andrew G. Leach [a, 1], Christopher R. Coxon [a, 2], Amos A. Fatokun [a], Darren W. Sexton [a], Iftikhar Khan [a], Georgios Zouganelis [a, 3], James Downing [a], Stefano Pluchino [b], Muttuswamy Sivakumaran [c], Meritxell Teixido [d], Touraj Ehtezazi [a, *]

[a] School of Pharmacy and Biomolecular Sciences, Liverpool John Moores University, Byrom Street, Liverpool L3 3AF, UK
[b] Department of Clinical Neurosciences, Clifford Allbutt Building - Cambridge Biosciences Campus and NIHR Biomedical Research Centre, University of Cambridge, Hills Road, CB2 0HA Cambridge, UK
[c] Department of Haematology, Peterborough City Hospital, Edith Cavell Campus, Bretton Gate Peterborough, PE3 9GZ, Peterborough, UK
[d] Institute for Research in Biomedicine (IRB Barcelona), Barcelona Institute of Science and Technology (BIST), Baldiri Reixac 10, Barcelona 08028, Spain

ARTICLE INFO

Article history:
Received 20 October 2020
Revised 3 December 2020
Accepted 7 December 2020
Available online 15 December 2020

Keywords:
MMP-9
Brain drug delivery
Self-assembled nanoparticles
BBB model
Peptides
Personalised medicine

ABSTRACT

This study investigated whether the inclusion of a matrix metalloproteinase-9 (MMP-9) responsive sequence in self-assembled peptide-based brain-targeting nanoparticles (NPs) would enhance the blood-brain barrier (BBB) penetration when MMP-9 levels are elevated both in the brain and blood circulation. Brain-targeting peptides were conjugated at the N-terminus to MMP-9-responsive peptides, and these were conjugated at the N-terminus to lipid moiety (cholesteryl chloroformate or palmitic acid). Two constructs did not have MMP-9-responsive peptides. NPs were characterised for size, charge, critical micelle concentration, toxicity, blood compatibility, neural cell uptake, release profiles, and *in vitro* BBB permeability simulating normal or elevated MMP-9 levels. The inclusion of MMP-9-sensitive sequences did not improve the release of a model drug in the presence of active MMP-9 from NPs compared to distilled water. ^{19}F NMR studies suggested the burial of MMP-9-sensitive sequences inside the NPs making them inaccessible to MMP-9. Only cholesterol-GGGCKAPETALC (responsive to MMP-9) NPs showed <5% haemolysis, <1 pg/mL release of IL-1β at 500 μg/mL from THP1 cells, with 70.75 ± 5.78% of NPs crossing the BBB at 24 h in presence of active MMP-9. In conclusion, brain-targeting NPs showed higher transport across the BBB model when MMP-9 levels were elevated and the brain-targeting ligand was responsive to MMP-9.

Introduction

Neurodegenerative diseases (NDs) have devastating effects on the quality of life and socio-economic status of sufferers and potentially lead to permanent disability.[1,2] NDs include: Alzheimer's disease and other forms of dementia, multiple sclerosis, Parkinson's disease, motor neuron disease, Huntington's disease and ataxia.[3,4] NDs are age-dependent and progressively widespread (Europe and US), in part because of increasing average life expectancy.[3,5] In the UK, dementia alone costs £26.3 billion a year.[6]

Numerous invasive (intrathecal/intracerebral ventricle route)[7,8] and non-invasive techniques have been employed to gain access to the brain such as chemical modification of drug molecules, physical disruption of the blood-brain barrier (BBB) or use of BBB shuttle peptides.[9,10] However, nanotechnology has gained significant attention in the past decade for the delivery of drugs across the BBB.[11–14] Polymeric nanoparticles (NPs),[15] liposomes,[16] exosomes,[17]

* Corresponding author.
E-mail address: t.ehtezazi@ljmu.ac.uk (T. Ehtezazi).
[1] Current address: School of Pharmacy, University of Manchester, Manchester, UK.
[2] Current address: Institute of Chemical Sciences, School of Engineering and Physical Sciences, Heriot-Watt University, Edinburgh, EH14 4AS.
[3] Current address: College of Life and Natural Sciences, University of Derby, Derby, DE22 1 GB, UK.

https://doi.org/10.1016/j.xphs.2020.12.004
0022-3549/

dendrimers,[18] and metallic NPs[19] have been explored for brain drug delivery.

Linear and branched THRre (PWVPSWMPPRHT) peptides have been developed for crossing the BBB through binding to the transferrin receptor.[20] It was found that branched THRre peptides showed a 2.6 fold increase in permeability compared to the original unbranched THRre peptide.[20] Apolipoprotein E (Apo E, residues 141−150), which binds with low-density lipoprotein (LDL) has been extensively explored for brain drug delivery to treat mucopolysaccharidosis type I, the most common lysosomal storage disorders with central nervous system deficits.[21,22] In another study, the 29-mer (YTIWMPENPRPGTPCDIFTNSRGKRASNG) of rabies virus glycoprotein (RVG) has been used to transport drug molecules and siRNA across the BBB.[23] RVG peptide binds specifically to the acetylcholine receptor (nAchR).[23] sRVG (CDIFTNSRGKRA), a 12-mer of RVG, was developed to bind with nAchR, which is able to cross the BBB.[24] Recently, MiniAP-4 (H-[Dap]KAPETALD-NH_2), a protease-resistant venom-derived peptide, was able to cross the BBB with minimum toxicity and immunogenicity.[25] These are only a few examples of the wide range of peptide-based brain-targeting ligands.

After crossing the BBB and entering the basal membrane, NPs may return to the blood.[26] Alternatively, matrix metalloproteinase 9 (MMP-9)-responsive NPs may provide drug delivery to the brain via a 'lock-in' mechanism; once the NPs/drugs cross the BBB, they undergo biotransformation leading to metabolites that are unable to cross back into the blood.[27] Of particular relevance here is, when MMP-9 levels are elevated in the brain in diseases such as traumatic brain injury[28] and multiple sclerosis.[29] The lock-in mechanism approach has also been taken for the delivery of L-dopa to the brain through prodrugs crossing the BBB.[30]

Within the fabrication procedures of NPs, self-assembly of NPs appears relatively straightforward compared to the other methods of NP production, which require sonication or use of organic solvents. In the self-assembly procedure, usually, an aqueous solution of the active ingredient is added to a solid powder of the amphiphilic compound and simply the dissolution of the powder by stirring/shaking is sufficient to dissolve the powder, leading to the formation of NPs and encapsulation of the active ingredient. Self-assembly can be defined as a process by which NPs or other components spontaneously organise themselves into thermodynamically stable structures.[31] This is associated with a thermodynamic equilibrium due to the balance between the amphiphilic components themselves and the interaction with their environment.[32] Therefore, the self-assembled NPs may provide a method to achieve a desired personalised medicine for the treatment of brain diseases.[33] Conceptually, a solution containing specific amounts of active ingredients can be readily prepared based on the severity/type of the brain disease in the patient. This solution can be added to the amphiphilic powder in the clinic for the formation of NPs followed by the administration of the NPs to the patient.

In this study, we have investigated whether the presence of an MMP-9 sensitive sequence would improve the ability of self-assembled peptide-based NPs to cross the BBB when levels of MMP-9 are elevated in the brain. To answer this question, we designed peptide constructs comprising a BBB targeting/penetrating peptides [(sRVG, CDIFTNSRGKRA),[24] (Apo E, LRKLRKRLLR)[34,35] or (MiniAP-3, CKAPETALC)[25]], which was conjugated at the N-terminus with an MMP-9 sensitive peptide sequence. Then, this peptide sequence was conjugated at the N-terminus with a fatty acid [cholesteryl chloroformate (CHF) or palmitic acid (PA)]. The hydrophobic group was attached to facilitate the self-assembly in the aqueous medium and to form NPs (schematically shown in Fig. 1). The NPs were characterised in terms of size, morphology, surface charge, cell toxicity, blood compatibility, neural cell uptake, and crossing an *in vitro* BBB model in the presence of active MMP-9. It was found that the existence of an MMP-9 cleavable sequence in the construct of the amphiphilic peptide (**AP**) increased permeation of the BBB model in the presence of active MMP-9. This was more significant, when the brain targeting ligand was itself sensitive to MMP-9. To our knowledge, peptide-based self-assembled brain-targeting MMP-9-responsive NPs have not been developed and this study provides an exciting new approach.

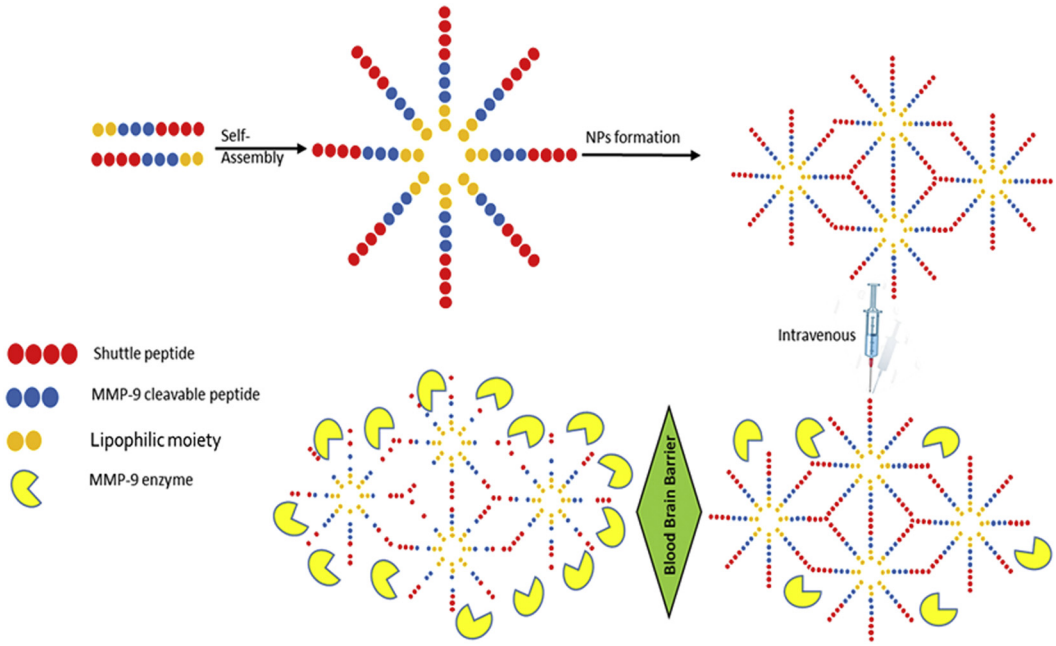

Fig. 1. Schematic presentation of self-assembly of MMP-9-responsive brain-targeting amphiphilic peptide-based constructs.

Materials and Methods

Materials

All Fmoc L-amino acids, Oxyma and ProTide® Rink Amide resin were purchased from CEM UK. N,N′-diisopropylcarbodiimide (DIC), piperidine, cholesteryl chloroformate (CHF), trifluoroacetic acid (TFA), triisopropylsilane (TIPS), acetonitrile, formic acid, N,N-diisopropylethylamine (DIPEA), 1(-2-Pyridylazo-2-napthol), pentane, Brij 35, Drabkin's reagent, FITC-dextran (molecular weight of 70 kDa) and pyrene were bought from Sigma-Aldrich. Fmoc-L-4-fluorophenylalanine was purchased from Fluorochem® (Hadfield, UK). Dimethylformamide (DMF), 1-(2-pyridylazo)-2-naphthol (PAN), fluorescein sodium salt (FSS) and diethyl ether (DEE) were purchased from Acros Organics®. MMP-9 recombinant human protein, His Tag (10327H08H5) was bought from ThermoFisher Scientific®. Dulbecco's Modified Eagle Medium (DMEM), fetal bovine serum (FBS), L-Glutamine, FAM-tagged negative siRNA, N-(3- Aminopropyl) methacrylamide hydrochloride (APMA) and antibiotic-antimycotic (anti-anti) were purchased from Sigma-Aldrich. Immortalised hCMEC/D3 cells were purchased from Merck EMD Millipore Corporation (28,820 Temecula, USA.).

Methods

Peptide Synthesis

Peptides were synthesised by solid phase peptide synthesis (SPPS) using a CEM Liberty Blue® automated microwave-assisted peptide synthesiser.[36] SPPS utilized Rink Amide resin (147 mg; loading capacity 0.61 mmol/g), standard Fmoc-deprotection (20% piperidine in DMF for 90 s at 90 °C), DIC (1 M) and Oxyma (1 M) solutions in DMF as activator and coupling reagents, respectively, and the required Fmoc-protected amino acids (0.2 M solutions in DMF), which were single coupled at 90 °C, except for Cys (50 °C) and Arg (double coupled at 75 °C). Peptides were cleaved from the resin by treatment with 1−2 mL of cleavage cocktail (trifluoroacetic acid: water: triisopropylsilane, 90%: 5%: 5%) for 4 h at room temperature and the solution was then filtered into cold diethyl ether, which precipitated the peptide. Precipitated peptide was washed and centrifuged with further diethyl ether four times to ensure the complete removal of impurities. Diethyl ether was evaporated by leaving it overnight in the fridge. Peptides were dissolved in distilled water and flash frozen (using liquid nitrogen) and lyophilised using a BUCHI Lyovapor L-200. Pilot studies indicated that the purity was >80% for short peptides, therefore, the synthesised peptides were not purified.

Conjugation of Cholesteryl Chloroformate (CHF) and Palmitic Acid (PA)

Pro-Tide resin-bound peptide (1 eq. based on loading capacity 0.61 mmol/g) was added to a solution containing cholesteryl chloroformate (CHF)/palmitic acid (2 eq.) and DIPEA (4 eq.) in DMF (4 mL) at 40 °C. The Kaiser test was performed to assess the conjugation completion and the process was repeated until complete coupling was indicated. In the case of palmitic acid (PA) conjugation, PA (10 mg/mL in DMF: DCM 50:50 *v/v* mixture) was activated by pre-treating with 50 μL of DIC for 30 min at room temperature.[37,38]

Characterization of Peptides by Liquid Chromatography-Mass Spectrometry

All of the peptides synthesised were characterised by using liquid chromatography-mass spectrometry (LC-MS) (Waters 2695 Separation Module linked with Quattro Premier Micromass) employing XBridge® Peptide BEH C18 column (130 Å, 5 μm and 4.6 mm × 150 mm). Samples were prepared in a mixture of water, acetonitrile and formic acid (80%: 20%: 0.1%) with an injection volume of 20 μL. A gradient separation technique utilized two mobile phases (A-water: formic acid 99.9%: 0.1%, B-methanol: formic acid; 99.9%: 0.1%).

NMR Studies

NMR studies were conducted by using the Bruker® Ascend™ 600 MHz NMR spectrometer. One-dimensional (1D) ^{19}F NMR (564.7 MHz) experiments were performed with proton decoupling at room temperature (298 K). A sample of MMP-9 responsive peptide, TY-11 (5 mg/mL, 350 μL), or ^{19}F labelled NPs was added to an NMR tube along with 400 μL of the activated MMP-9 in TCNB buffer. Peptide products and degradants containing 4-fluorophenylalanine were observed as singlets with different characteristic chemical shifts. Chemical shift values were calibrated to TFA (−76.55 ppm) as the internal standard. Data obtained was viewed and analysed by using the TopSpin® software.

Dynamic Light Scattering (DLS)

Particle size and zeta potential were measured by applying the dynamic light scattering (DLS) technique using Malvern Zetasizer Nano ZS® (Malvern, Worcestershire, UK). Cuvettes used were DTS0012 from Malvern. **AP**s were dissolved/dispersed in water and sizes were measured with a delay time of 2 min. Sample was stabilized for 120 s before measurement.

Scanning/Transmission Electron Microscopy (SEM/TEM)

NPs were visualized and characterised morphologically by FEI Morgagni transmission electron microscopy. Carbon filmed copper grids were used. NP solution (2.5 mg/mL) was prepared in distilled water. A small droplet of the **AP** solution was placed on the grid and left for drying in a fume hood and no staining (negative or positive) was used. NPs were observed by using the FEI Inspect S (Oxford-instrument) at an accelerating voltage of 100 kV. For scanning electron microscopy (SEM), the sample was coated with gold using an Emitech K550 (Ashford, UK) coater and then visualized with a Philips XL20 (Eindhoven, Holland) scanning electron microscope.

Critical Micelle Concentration (CMC) Determination

Two different techniques were used to determine the critical micelle concentration (CMC), using PAN[39] and pyrene.[40] Using PAN procedure, CMCs were determined by employing a Genesys® 6 UV/Vis spectrophotometer. A volume of 20 mL **AP** solution was prepared at 0.5 mg/mL. Then **AP** solution was serially diluted from 0.01 to 0.3 mg/mL with saline (0.9%) in volumetric flasks. The **AP** solutions were shaken to ensure **AP** and saline solution is thoroughly mixed. PAN was used as a probe and dissolved in pentane at the final concentration of 1.6 mM. PAN (500 μL) solution was added into each volumetric flask containing **AP** solution. Samples were left for 30 min for the evaporation of pentane in the fume hood. After complete removal of pentane, UV absorbance was determined at wavelength of 470 nm.

For validation, the CMC was also measured for each formulation using pyrene.[40] Initially, a pyrene solution was prepared in acetone at a concentration of 6.16×10^{-7} M. Next, volumetric flasks were each filled with 20 mL of the pyrene solution and placed in a water bath at 80 °C to allow rapid evaporation of the acetone and deposition of pyrene. A stock solution of **AP** was then prepared at a known concentration. Once acetone had been evaporated, flasks were removed from the water bath and the **AP** solution was then added at a range of concentrations to each individual flask containing pyrene and shaken thoroughly. The samples were then placed in an oven at 35 °C for 24 h ensuring equilibration. After 24 h, the samples were removed from the oven and analysed using

the fluorescence spectrometer (Varian Cary Eclipse). The intensity of each solution was recorded (I335 and I320).

Absorbance or intensity were then plotted onto a graph (depending on technique) against concentration. The position of a significant and continuous increase in absorbance or intensity was taken as the CMC.

Encapsulation Efficiency

The encapsulation capacity of NPs was calculated by an indirect method.[41] Briefly, FSS solution (1 mL of 0.09 μg/mL in distilled water) was transferred into an Eppendorf tube containing 3 mg of **AP** powder. Upon contact with water, **AP**s self-assembled into NPs encapsulating the FSS (model drug) without any sonication.

The solution (450 μL) was transferred into cellulose centrifugal filter units (Amicon Ultra 0.5 mL 3K, Merck Millipore Ltd.) and centrifuged for 10 min at speed of 10,000 RPM. The filtrate was then transferred to a clear falcon 96 well plate and the fluorescence was measured using a SpectraMax i3X multi-mode microplate reader at excitation wavelength of 460 nm and emission at 515 nm. The encapsulation efficiency was calculated by using the equation derived from a calibration curve. Each experiment was performed four times (n = 4).

MMP-9 Activation Protocol

MMP-9 was activated in TCNB buffer (50 mM Tris, 10 mM $CaCl_2$, 150 mM NaCl, 0.05% Brij35, pH 7.5) following the manufacturer's instruction. Firstly, the TCNB buffer was prepared and pH was adjusted to 7.4. Then 5 μg of MMP-9 was suspended in 50 μL of the TCNB buffer (100 μg/mL) and incubated for 24 h with (APMA) to a final concentration of 1 mM at pH of 7.4. The mixture was diluted to a concentration of 2 nM and aliquoted.

Release Studies

AP (3 mg) was transferred into an Eppendorf tube to which 1 mL of FSS solution (0.09 μg/mL in distilled water) was added and the sample was mixed gently by hand. Then, the NP solution (1 mL) was transferred to a dialysis bag (cellulose with a diameter of 1 inch and with molecular weight cut-off 10,000 Da MWCO) with 1 mL of the external stimuli (total 2 mL inside the bag). The external stimuli was one of the following media: fetal bovine serum (FBS) solution, distilled water, BSA (4 mg/mL), NaCl (0.9%), Glucose (7.8 mM as normal body level), activated MMP-9 (2 nM) and Dioralyte, which is an oral rehydrating solution containing glucose 3.56 g/200 mL (18 mM), NaCl 0.47 g (12 mM), potassium chloride 0.30 g (4 mM), and disodium hydrogen citrate 0.53 g (2 mM). The dialysis bag with molecular weight cut-off 10,000 Da MWCO was chosen to prevent the infiltration of proteins (MMP-9 or BSA) and/or NPs from the bag, which was dialysed against 40 mL of distilled water. A sample was withdrawn every hour from the external compartment (outside of the bag) and returned after measurement. Each experiment was performed in triplicate. For comparison, FSS release was also measured from the dialysis bag with the external stimuli only (as listed in the above), i.e. without NPs.

In Vitro Toxicity

The lactate dehydrogenase (LDH) assay was used to assess the potential toxicity of the NPs. HeLa and SH-SY5Y cells were grown in T25 or T75 flasks, using Dulbecco's Modified Eagle Medium (DMEM) supplemented with 10% FBS and 2 mM L-glutamine. They were incubated at 37 °C in a humidified atmosphere of 5% CO_2. When they had attained between 80 and 90% confluency the cultures were rinsed with phosphate-buffered saline, trypsinised, re-suspended in the growth medium, counted and seeded into an opaque, micro-clear, flat bottom 96 well tissue culture plate at a density of 7.5×10^4 cells/mL (7500 cells/well at 100 μL/well). The 96 well plate was then incubated overnight at 37 °C with a 5% CO_2 supply. The NPs were prepared in sterile distilled water and then added to the culture wells in triplicate. Dimethyl sulfoxide (DMSO) 5% was added to the positive control wells, and vehicle only to the negative control wells. The treated 96 well plate was then incubated for 24 h at 37 °C/5% CO_2/humidified air, at the end of which, the LDH assay was carried out according to the manufacturer's protocol (ThermoFisher, Pierce LH Cytotoxicity Assay Kit, Cat. No. 88953) and as recently reported.[42]

The MTT (3-(4,5-Dimethyl-2-thiazolyl)-2,5-diphenyl-2H-tetrazolium bromide) assay was employed to assess the effects of treatments on cell viability using the Vybrant®MTT cell proliferation assay kit (Thermo Fisher Scientific, USA) according to the manufacture's instruction. After treatment of the cells with the NPs (prepared in sterile distilled water), MTT was added to each experimental well and the plate was incubated for 3 h. The supernatant was aspirated carefully, and the blue crystals of formazan were dissolved using DMSO, with plate shaken gently for 5 min while covered in foil to protect it from light. The absorbance was then measured at 570 nm on a plate reader (CLARIO star from BMG Labtech).

Three different concentrations (0.0469, 0.1875 and 0.75 mg/mL) were examined for selected **AP**s. All experiments were performed three independent times (n = 3) in triplicate (i.e. each in triplicate wells).

In Vitro Cellular Uptake/Flow Cytometry

To assess the *in vitro* cellular uptake, SH-SY5Y cells grown in DMEM media were seeded into a 24-well plate at a density of 5000 cells/well. The plates were incubated at 37 °C in a humidified atmosphere of 5% CO_2 until desired confluency (80% after two days incubation) was achieved. Cells were treated with two formulations (dispersed in RNAse free water and encapsulating FAM-siRNA) at a concentration of 0.3 mg/mL. The cells were incubated for 4 h, as reported previously.[43] Then, cells were washed with phosphate buffer (PBS) three times to remove the formulation and FAM-siRNA. Trypsin (100 μL) was added to each well to detach the cells from the surface. Trypsin was decanted and plates were incubated. DMEM medium (200 μL) was added to each well, and the well content was mixed by pipetting up and down. Cellular uptake was analysed by BD Accuri™ C6 Plus flow cytometer containing 488 nm and 640 nm lasers with fluorescence detection of FAM positive viable cells assessed using the FL-1 detector (λ_{ex} 488 nm; λ_{em} 533/30 nm). In terms of data analysis, debris and dead cells were gated out of the analysis.

Confocal Microscopy

To visualise the cellular uptake, confocal microscopy was performed by using Zeiss LSM 780 confocal microscopy system (Carl Zeiss Meditec AG, Jena, Germany). FAM-siRNA solution (500 nM) was prepared in nuclease free water. **AP** powder (10 mg) was mixed with 1 mL of FAM-siRNA solution (0.5 PMOL/μL) without any sonication. The self-assembly of the NPs facilitated the encapsulation of FAM-siRNA. hCMEC/D3 cells were seeded into 4 chambered glass slides at a density of 30,000 cells/well. Cells were incubated for 2 days and desired confluency was achieved. It was observed in preliminary experiments that hCMEC/D3 cells at certain density took specific time to get to a suitable confluency. The cell confluency of 60–80% was usually required as 100% confluency affected the visibility in confocal microscopy. **APs** were added to wells (0.3 mg/mL concentration of **AP** in each containing cells) and incubated for 24 h. Cells were washed three times with PBS. Cold methanol (600 μL) was added to the wells of the slide, which subsequently was placed in the freezer for 10 min. Methanol was decanted and cells were washed with PBS (2–3 times). DAPI

(100 nM) solution (500 μL) was added to each well and left for 10 min. DAPI was decanted and washed with PBS 2–3 times and was left to dry. Three to four drops of mounting media were added and sealed using a cover slip. The slide was visualized under the confocal microscope.

Electrophoresis

The complex formation of FAM-siRNA with **AP**s was studied using an agarose gel retardation electrophoresis assay.[44] Briefly, 1% gel was cast in the mould (1.5 g of agarose was dissolved in 100 mL of Tris/Borate/EDTA (TBE) buffer by boiling). Red dye (GelRed) 2 μL was added to the solution, which was left to cool. Then the sample was added into each well (8 μL of **AP** + FAM-siRNA with 3 μL of loading dye (bromophenol blue and xylene cyanol FF)). Electrophoresis was performed at 70 mV for 20 min. The gel was analysed with a Biorad spectrophotometer. Also, FAM-siRNA was dissolved in 100 μL of PCR quality water, then 5 μL was diluted in 495 μL of PCR quality water. **AP** solution (1 mg/mL) was also prepared in PCR grade water. Serial dilutions were prepared with **AP** and FAM-siRNA solution.

In Vitro BBB Permeability

The BBB *in vitro* model was constructed using a protocol supplied by Merck Millipore as also reported in our previous work.[42] *In vitro* permeability across the monolayer of neural cells was performed using immortalised hCMEC/D3 cells. The immortalised cell line has been extensively characterised for brain endothelial phenotype and is a model of human BBB function. hCMEC/D3 cells were seeded (90,000 cells/insert) in Sarstedt transwell inserts (PET 0.4 μm, TP). Cells were cultured using EndoGRO media (SCME004) supplemented with hydrocortisone, ascorbic acid, heparin sulfate, rhEGF, L-glutamine, EndoGro-LS supplement and 5% FBS. A tissue culture (TC) insert was placed in each well of a 24-well plate containing 1.6 mL of pre-warmed culture media (37 °C, the basolateral compartment). After 24 h of incubation, transepithelial/endothelial electrical resistance (TEER) was measured by using EVOM[2] (World Precision Instruments, Sarasota, Florida, USA). The apical compartment (300 μL) content was replaced every 24 h with fresh media. At the highest TEER values, NP formulations (encapsulated with FAM-siRNA, as described in section Confocal Microscopy) were added to the apical compartment to the final desired concentration (0.380 mg/mL except **AP-6**:0.200 mg/mL). Fluorescence in the basolateral compartment was measured at every hour using SpectraMax i3X multi-mode microplate reader (Molecular Devices, USA) at an excitation wavelength of 460 nm and at an emission wavelength of 495 nm. Additional experiments were conducted in the presence of active MMP-9 with 140 ng/mL in the basolateral compartment simulating diseased brain (bacterial meningitis CSF MMP-9 concentration range: 2.55–365 ng/mL),[45] and with 0 ng/mL, 50 ng/mL, and 100 ng/mL in the apical compartment, simulating serum levels of the healthy (40.8 ± 12.9 ng/mL)[46] and diseased individuals, such as multiple sclerosis (125 (36–376) ng/mL).[45] TEER values were measured following using MMP-9 in the BBB model for 100 ng/mL in the apical compartment and 140 ng/mL in the basolateral compartment. Following treating hCMEC/D3 cells in the TC inserts with NPs and MMP-9 (50 ng/mL in the apical compartment and 140 ng/mL in the basolateral compartment) for 24 h, cells were carefully washed with PBS and pre-warmed media was added. TEER values were measured again and media were replaced with pre-warmed fresh media. Then, 10 μL of FITC-dextran solution (1 mg/mL) was added to the TC insert and fluorescence (λ_{exc} 485 nm, λ_{ems} 520 nm) was measured in the basolateral compartment every hour for 6 h. The transmigration of NPs across the BBB and apparent permeability (P_{app}) were calculated as reported previously.[42,47]

The permeability of BBB monolayer was tested against unencapsulated (naked) FAM-siRNA by using histamine and cimetidine. Briefly, cells were seeded at 90,000 cells/insert and after 24 h media were replaced and histamine was added into inserts at a final concentration of 50 μM. The plate was incubated at 37 °C for 12 h and then FAM-siRNA at the concentration of 125 nM was added to the apical compartment and the fluorescence of FAM-siRNA was measured in the basolateral compartment every hour for 6 h.

In another set, as above, cells were seeded at 90,000 cells/insert and after 24 h media were replaced and histamine was added into inserts at a final concentration of 50 μM. Then cells were washed with sterile PBS buffer, but this time cimetidine was added into inserts at a final concertation of 50 μM. The plate was incubated for 1 h and then FAM-siRNA at the concentration of 125 nM was added to the apical compartment and the fluorescence of FAM-siRNA was measured in the basolateral compartment every hour for 6 h.

Each experiment was performed three independent times in triplicate (i.e. each in triplicate wells).

Haemolysis

All human blood samples were drawn from healthy volunteers and used with the institutional (Liverpool John Moores University) bioethics approval and informed consent was obtained from three donors prior to phlebotomy. All donors did not have a previous history of any major disease and did not take anti-platelet agents such as aspirin, or anti-inflammatory medications such as ibuprofen along with no history of smoking. Citrated blood was obtained from the donors (one donor for each separate run of experiment); and three blood samples were representatives of three independent experiments and individual blood types.

The haemolysis assay had two parts. In the first part, it was evaluated that whether plasma-free haemoglobin (PFH) was less than 1 mg/mL, indicating that red blood cells were intact. The assay was based on quantitative determination of red-coloured cyanmethemoglobin of total haemoglobin in the whole blood (TBH) and PFH.[48,49] An increase in the PFH is indicative of haemolysis and release of the haemoglobin which is oxidized to methemoglobin. Drabkin's solution (cyanmethemoglobin reagent, including cyanide) was added to the whole blood sample to lyse erythrocytes and estimate TBH. In contrast, its addition to plasma was used to detect PFH by converting methemoglobin to its stable form (cyanmethemoglobin form), which was detectable by spectrophotometry at 540 nm.[48] Briefly, the supernatant of the blood sample (centrifuged 15 min at 800×*g*) was used to determine PFH. Known haemoglobin concentrations in the range of 0.025 mg/mL to 0.8 mg/mL were used to prepare a standard curve. In a 96-well plate the following solutions were add: three quality control samples, 200 μL of calibration standard, quality controls and blanks. TBH sample (200 μL, prepared by combining 20 μL of the whole blood and 5.0 mL of cyanmethemoglobin reagent) and PFH (100 μL) were added to six wells of the 96-well plate. Finally, 100 μL of cyanmethemoglobin (CMH) reagent was added to each well containing PFH. Having been covered with a plate sealer and shaken for 1–2 min, plate absorbance at 540 nm (measured by CLARIOSTAR microplate reader) led to haemoglobin standard curve and TBH concentration determination.[50] As the PFH levels were less than 1 mg/mL for all three donors, then the next part of the assay was conducted as the following.

Citrated blood samples were diluted with Ca^{2+}/Mg^{2+}-free PBS to adjust the TBH concentration to 10 ± 2 mg/mL (TBHd).[49] In two racks of Eppendorf tubes, 100 μL of each NP sample in four concentrations (50, 100, 250, 500 μg/mL), blank, positive control (Triton X-100 1%) and negative control (sterile normal saline) was added to each tube. TBHd (100 μL) was then added to only one of the racks and another rack represented “no blood” controls to

evaluate potential interference of the NP materials with the assay. Finally, Ca^{2+}/Mg^{2+}-free PBS was added in each tube up to a total volume of 900 μL, followed by incubating at 37 °C for 3 h ± 15 min and mixing the samples every 30 min. Then, the mixture was centrifuged at 800×*g* for 15 min. Known haemoglobin concentrations in the range of 0.025−0.8 mg/mL were used to prepare a standard curve.

To a fresh 96 well-plate, 200 μL of blank reagent, calibrators (calibration standard), and quality controls were added in respective wells. Then, 100 μL supernatant of a centrifuged sample (NP or control) with 100 μL of CMH reagent (prepared by mixing 1000 mL Drabkin's reagent and 0.5 mL of 30% Brij 35 solution) were added to one well of the plate (six wells for each NP concentration). TBHd sample (200 μL, diluted by combining 400 μL of the TBHd and 5.0 mL of CMH reagent) was added to six wells. Finally, a volume of 100 μL CMH reagent was added to each well containing NPs or controls. Having been covered with a plate sealer and shaken for 1−2 min, plate absorbance at 540 nm was measured using CLARIOSTAR microplate reader (BMG Labtech, Offenburg, Germany), which led to haemoglobin standard curve and haemoglobin concentration determination.[50]

After applying a dilution factor of 18 for samples and controls and a dilution factor of 13.5 for TBHd, the percentage of haemolysis was calculated from Equation (1):

$$\frac{Haemoglobin\ in\ Test\ Sample}{TBHd} x100\% \quad (1)$$

A percentage of haemolysis <2 means the NP sample is not haemolytic; 2−5% haemolysis indicates the test sample is slightly haemolytic; and >5% haemolysis implies the formulation is haemolytic.[48,49] Also, examining centrifuged tubes for unusual appearance is essential to avoid false-positive and false-negative interference. Moreover, inhibition/enhancement controls helped to exclude false-negative results. False-positive interference due to overlapping of NP optical density with the assay wavelength was ruled out by NP-only blood-free controls.[48] The experiments were performed in triplicate (i.e. each in triplicate wells).

IL-1 β Analysis

The THP1 cell line was maintained at 2 × 10^5 cells/mL (cultured in RPMI 1640 medium supplemented with 10% FBS and antibiotics) and incubated with NP solution (in concentrations of 100, 250 and 500 μg/mL), positive control (10 ng/mL and 100 ng/mL of lipopolysaccharide) and negative control (medium) for 20 h followed by harvesting (centrifugation 5 min at 350 g) and storing supernatants at −80 °C until analysis of IL-1β level by ELISA (Thermo Fisher).[51] Uncoated ELISA protocol was performed according to the manufacture's instructions. In brief, this entails coating ELISA plate with capture antibody and incubating overnight at 4 °C followed by washing 3 times. Then, wells were blocked with ELISA/ELISPOT Diluent and 2-fold serial dilutions of the top standards were performed to create the standard curve (in the range of 2−150 pg/mL of IL-1β). A volume of 100 μL/well of NP treated samples was added to the respective wells and incubated overnight at 4 °C. Following washing, the plate was incubated with detection antibody for 1 h at room temperature and again washed 3 times. Finally, enzyme (Avidin-HRP) was added and the plate was incubated for 30 min at room temperature. This was followed by washing 5 times the well (with the wash buffer) and the addition of 100 μL/well substrate solution (TMB solution). After 15 min incubation at room temperature, 50 μL of the stop solution was added to each well. The absorbance was measured at wavelength of 450 nm, and each value was subtracted from the absorbance at 570 nm.[52] The absorbance was measured using CLARIOSTAR microplate reader (BMG Labtech, Offenburg, Germany). All experiments were performed three independent times (n = 3) in triplicate (i.e. each in triplicate wells).

Statistical Analysis

GraphPad Prism Software 8.0.1 for Windows (GraphPad Software, Inc., La Jolla, CA, USA) was used to conduct one-way analysis of variance (ANOVA) followed by Tukey's post-hoc test for multiple comparisons in order to identify any statistically significant differences between the treatment groups. For statistical comparisons, $P < 0.05$ was considered a statistically significant difference. All values are presented as mean ± SD.

Results

Synthesis of Amphiphilic Peptides

Following synthesis, LC-MS was performed to confirm the peptide identity based on mass/charge ratio (*m/z*) (Fig. S1, supplementary information). A summary of molecular weights of the peptides before and after conjugation are shown in Table 1 (the part of the sequences in bold are BBB targeting ligands). Table 1 starts with **AP-1** (C_{27}-WGPIA**LRKLR**) which was a low molecular weight amphiphilic compound (1621.36 Da) and then gradually increases to **AP-5** (C_{27}-GGGRPLGLW**CDIFTNSRGKRA**) with molecular weight of 2672.77 Da. These compounds had MMP-9 cleavable peptide sequences, apart from **AP-9**, which was synthesised as control compound. Our preliminary work (due to publication) discovered a novel MMP-9 cleavable peptide WGPIA and cleavability of MiniAP-3 (CKAPETALC) by MMP-9. Then constructs with MiniAP-3 did not include additional MMP-9 sensitive sequence. RPLGLW was an MMP-9 cleavable sequence reported previously.[53] Our studies indicated that WGPIA would have more sensitivity towards MMP-9 than RPLGLW. Therefore, we incorporated WGPIA in four compounds as MMP-9 cleavable sequence, as opposed to two compounds that contained RPLGLW sequence. The MMP-9 cleavable sequences are shown with red font in Table 1. All **AP**s had GGG as a

Table 1
Summary of Amphiphilic Peptide Descriptions.

Name	Sequence	M_{cacl} (g/mol) Before Conjugation (Da)	M_{cacl} (g/mol) After Conjugation (Da)	$[M + H]^+$	$[M + H]^{2+}$	$[M + H]^{2+}$ or $[M + H]^{2+}/2$
AP-1	C_{27}-*WGPIA***LRKLR**	**1208.75**	**1621.36**	**1622.36**	**1623.36**	**811.7438**
AP-2	C_{27}-GGG*WGPIA***LRKLR**	**1379.81**	**1792.42**	**1793.42**	**1794.42**	**896.21**
AP-3	C_{27}-GGG**CKAPETALC**	**1105.49**	**1518.1**	**1519.1**	**1520.1**	**759.05**
AP-4	C_{27}-GGGW**CKAPETALC**	**1291.57**	**1704.68**	**1705.68**	**1706.68**	**852.09**
AP-5	C_{27}-GGG*RPLGLW***CDIFTNSRGKRA**	**2260.16**	**2672.77**	**2673.77**	**2674.77**	**1337.385**
AP-6	C_{16}-GGG*RPLGLW***CDIFTNSRGKRA**	**2260.16**	**2496.57**	**2497.57**	**2498.57**	**1249.83**
AP-7	C_{27}-GGG*WGPIA***LRKLRKRLLR**	**2046.28**	**2458.89**	**2459.89**	**2460.89**	**1230.73**
AP-8	C_{16}-GGG*WGPIA***LRKLRKRLLR**	**2046.28**	**2282.69**	**2283.69**	**2284.69**	**1142.345**
AP-9	C_{27}-GGG**CDIFTNSRGKRA**	**1537.74**	**1950.35**	**1951.35**	**1952.35**	**976.056**

Italic font denotes MMP-9 cleavable sequence and bold font shows brain-targeting ligand.

Table 2
Characteristics of Self-Assembled Peptide-Based Brain Targeting NPs.

Formulation	Size (nm)[c]	Zeta Potential (mV)	CMC (mg/L)	PdI[a]	Construct Charge	Encapsulation Efficiency%
AP-1	111.66 ± 12.39	24.68 ± 3.87	100	0.22	3+	ND
AP-2	32.89 ± 17.17	22.9 ± 5.39	80	0.57	3+	67.72 ± 6.41
AP-3	81.4 ± 7.65	36.53 ± 1.37	40	0.43	1+	79.60 ± 3.36
AP-4	2796 ± 739.5	38.68 ± 2.14	15	0.99	1+	ND[b]
AP-5	726.03 ± 18.16	25.43 ± 0.33	7,50	0.39	3+	ND[b]
AP-6	72.60 ± 1.62	34.5 ± 4.36	75	0.43	3+	77.85 ± 4.16
AP-7	166.2 ± 62.76	16.5 ± 2.89	95	0.20	6+	75.53 ± 6.56
AP-8	104 ± 31.76	25.26 ± 0.64	90	0.44	6+	ND[b]
AP-9	293.7 ± 21.75	26.45 ± 6.72	82	0.63	3+	69.11 ± 4.24

Data represent mean ± SD.
[a] PdI: Polydispersity Index of a typical distribution.
[b] ND: Not Determined.
[c] SD represents the standard deviation of three average particle sizes.

linker between the MMP-9 sensitive peptide sequence and the hydrophobic moiety, except for **AP-1**.

Particle Size Distribution, Morphology and CMC

To assess the morphology and particle size of NPs, 2.5 mg/mL solution/suspension were prepared. Interestingly, peptide powder dissolved instantly with the addition of water giving a clear solution-like appearance, with the exception of **AP-4** and **AP-5**, which afforded a cloudy suspension. The size of **AP-5** NPs measured by DLS was more than 500 nm, whereas SEM revealed that the NPs were much smaller, mainly due to the agglomeration of particles. The summary of the particle size, zeta potential and CMC for the NPs are given in Table 2. The zeta potential for all NPs were in the range of 16−40 mV, independent of amphiphilic construct charge (Table 2). All average particle sizes were less than 200 nm except **AP-5** as shown in Table 2. Also, polydispersity index (PdI) values were less than 1 (Table 2).

In a typical DLS measurement, the particle size distribution spread beyond 200 nm (Fig. S2), but when TEM was performed, the particle size was less than 200 nm. Fig. 2 illustrates the shape of the NPs visualized by TEM or SEM. Most of the self-assembled NPs were found to be spherical. As **AP-4** and **AP-5** samples appeared cloudy with rapid settlement of the particles, therefore, these compounds were not further investigated. **AP-4** had only one extra tryptophan residue compared to **AP-3**; yet **AP-4** did not form NPs. While **AP-3** self-assembled to form distinct NPs. The rationale for addition of tryptophan to **AP-3** was to achieve NPs with rigid structure and resistant to disassembly in physiological solutions such as the

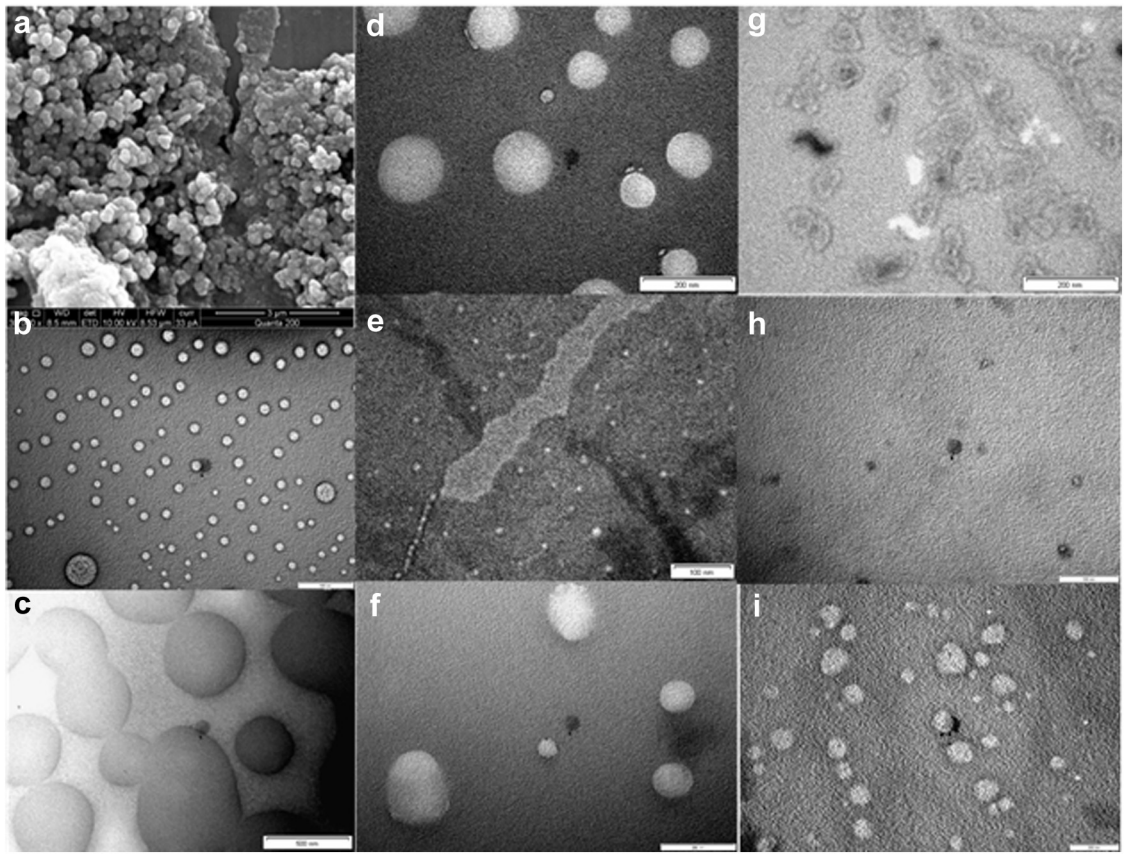

Fig. 2. Typical electron micrographs of unstained self-assembled peptide-based brain-targeting NPs at a concentration of 2.5 mg/mL. a) SEM image of **AP-5**, b) TEM image of **AP-6**, c) **AP-1**, d) **AP-2**, e) **AP-3**, f) **AP-7** g) **AP-4**, h) **AP-8** and i) **AP-9**.

blood, a phenomenon that may happen to self-assembled NPs after intravenous injection.

The CMCs of all the peptide formulations were in the range of 7−100 mg/L. CMC graphs are illustrated in the supplementary information (Figs. S3-S11). Also, it can be seen from Table 2 that the addition of tryptophan (W) to the peptide sequence of **AP-3** decreased significantly the CMCs for **AP-4** and as a result the particle size increased from 81.4 ± 7.65 nm for **AP-3** to 2796 ± 739.5 nm for **AP-4**.

Release Profiles in the Presence of MMP-9

The encapsulation efficiencies of FSS are given in Table 2 for **AP-2, AP-3, AP-6**, **AP-7,** and **AP-9** NPs. They were greater than 60%.

Fig. 3a−d presents release profiles of FSS from **AP-3**, **AP-6**, **AP-7**, and **AP-9**, respectively. It can be seen that release profiles changed in the presence of different stimuli. The release of FSS was 41.14 ± 0.48% of loaded dose for **AP-6** (Fig. 3b) in distilled water at 24 h. While, 90.49 ± 5.37% of FSS solution released from the dialysis bag at 24 h (Fig. 3e). These observations show that the self-assembled NPs were stable in water up to 24 h.

In the first hour, 13% of FSS was released from **AP-6** NPs compared to 31% of **AP-3** NPs. It may be suggested that the **AP-6** NPs had a dense matrix-like structure compared to **AP-3** NPs. All the formulations showed higher release of FSS in the presence of FBS compared to distilled water. This may be expected, as the presence of enzymes/peptidases in the FBS degraded the peptide-based NPs and hence accelerated the release of FSS compared to distilled water. Almost 100% of FSS was released after 24 h in the presence of FBS for both **AP-6** and **AP-3** NP formulations.

The release of FSS decreased from the NPs in the presence of BSA compared to distilled water for **AP-3**, **AP-6** and **AP-9** NPs, as shown in Fig. 3a, b, and d, respectively. Particle size distribution was measured for **AP-6** NPs in BSA solution (Fig. S12). NPs in distilled water had a size of 72.60 ± 1.62 nm and the particle size distribution was relatively narrow. However, particle size distribution increased (321 ± 6.281 nm) in the presence of BSA, suggesting the formation of protein corona and possibly NP aggregation. Therefore, the slow release of FSS in the presence of BSA could be partly due to the adsorption of BSA protein molecules on the surface of NPs and affecting the release of FSS.

Unexpectedly, the release of FSS was not faster in the presence of MMP-9 compared to distilled water, during the first 5 h (Fig. 3a−d). This finding would be expected for **AP-9**, which was synthesised as a control and did not contain an MMP-9 cleavable sequence. Faster FSS release had been expected compared to distilled water for **AP-3**, **AP-6** and **AP-7** as these contained MMP-9 cleavable peptide sequences in their constructs (for **AP-3**, the brain targeting ligand was sensitive to MMP-9). Release of only FSS was 90.94 ± 5.37% within 24 h in distilled water, while in the presence of TCNB (buffer used to activate the MMP-9) and BSA it dropped to 51.50 ± 2.94% and 23.22 ± 2.52%, respectively (Fig. 3e). Therefore, the buffer of the MMP-9 enzyme solution and proteins had retarding effects on the release of FSS compared to distilled water. Furthermore, it was found that the release of FSS in the presence of MMP-9 from NPs was in the order of **AP-2**> **AP-1**> **AP-3**> **AP-7**> **AP-9**> **AP-6** at 5 h (Fig. 3f). This trend shows that **AP**s with shorter peptide chain length showed higher sensitivity to MMP-9 compared to **AP**s with longer chains. **AP-3** NPs achieved the highest FSS release at 24 h (Fig. 3f).

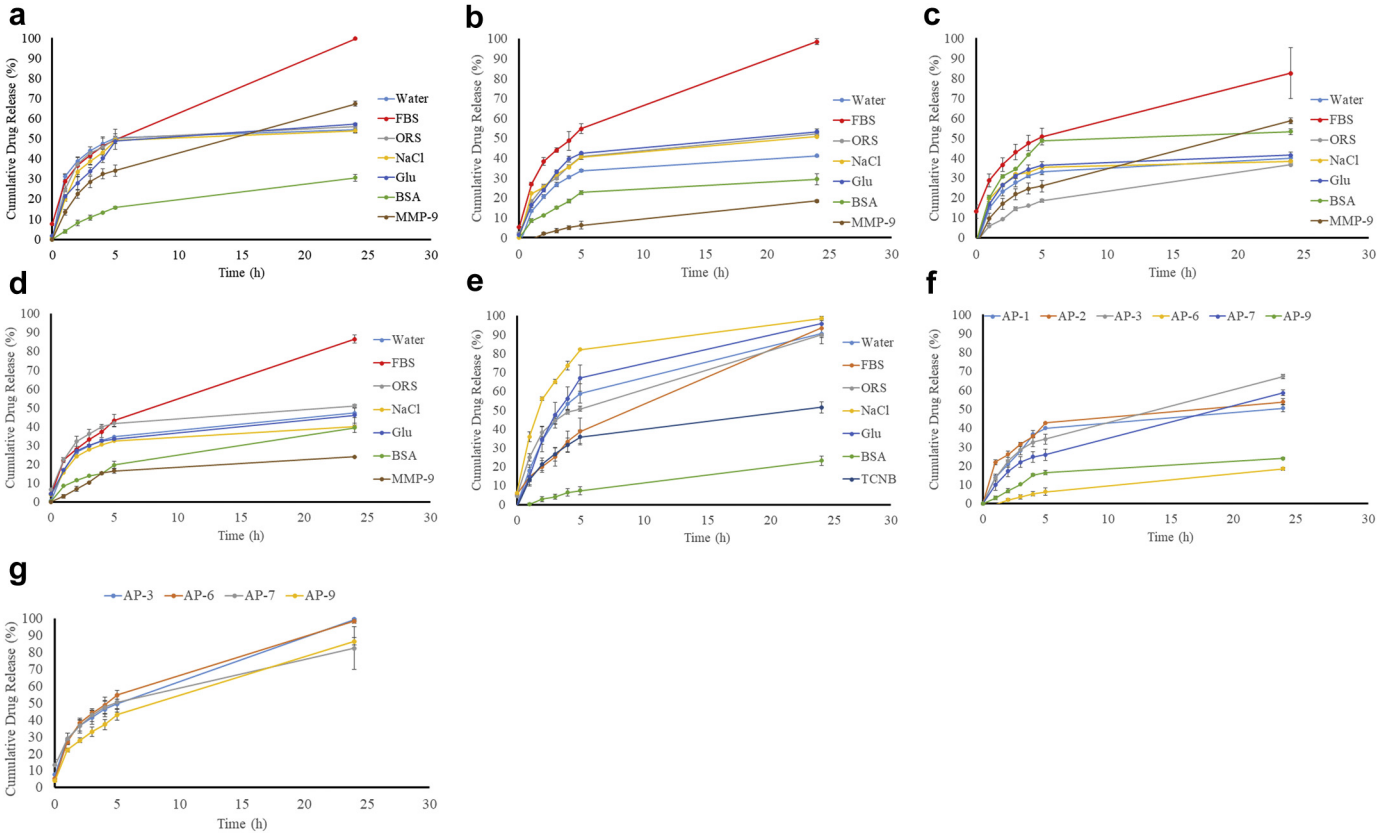

Fig. 3. Release profiles for enzyme-responsive self-assembled peptide-based brain-targeting NPs in the presence of different external stimuli and active MMP-9. a) **AP-3** b) **AP-6**, c) **AP-7**, d) **AP-9**, e) fluorescein sodium salt only, f) NPs in the presence of active MMP-9, g) NPs in the presence of FBS. Error bars show standard deviation and each experiment was run three independent times (n = 3).

To have an insight into the degradation kinetics of NPs in the presence of MMP-9, an analogue of **AP-5** was synthesised, which the phenylalanine at position 9 was replaced with 4-fluorophenylalanine (C_{27}-GGGRPLGLW**CDI**^{19}**FTNSRGKRA**) to install a ^{19}F NMR reporter. The construct was easily dissolved in aqueous media than the parent non-fluorinated analogue and formed NPs with an average size of 127.77 ± 2.28 nm and PdI of 0.28. These NPs were incubated with MMP-9 and proton-decoupled ^{19}F NMR spectra were obtained, however, the signal-to-noise ratio was poor (Fig. 4a) and did not change with time. On the other hand, an MMP-9 responsive peptide (PLGLWG^{19}FQ) exhibited significantly higher signal-to-noise ratio in the ^{19}F NMR at the same concentration. In addition, the signal changed with time in the presence of MMP-9 (Fig. 4b). These observations suggested that MMP-9 cleavable sequences might not have been available to MMP-9 and buried inside the NPs. This inference can be further supported by comparing the release profiles of **AP-2** and **AP-7** (Fig. 3f). **AP-2** showed a faster release compared to **AP-7** up to 5 h. The brain targeting ligand of **AP-7** (10 residues) was longer than **AP-2** (5 residues), suggesting that the MMP-9 cleavable sequence (WGPIA) became less accessible to MMP-9 in the **AP-7** construct. Furthermore, **AP-3** showed the highest amounts of FSS released at 24 h (Fig. 3f) in the presence of MMP-9, indicating that NPs became more sensitive to MMP-9 when the brain targeting ligand itself was sensitive to MMP-9. However, the NP formulations did not show difference in the release profiles in the presence of strong FBS enzymes (Fig. 3g).

In summary, inclusion of MMP-9 cleavable sequences increased the release rate (except **AP-6**); and the release rates increased further when brain targeting ligand was short and comparable to MMP-9 cleavable sequence (**AP-2**), or ultimately when the brain targeting ligand itself was responsive to MMP-9 (**AP-3**).

Cell Toxicity of NPs

In vitro toxicity of self-assembled NPs was tested on SH-SY5Y cells using both LDH (Fig. 5a) and MTT (Fig. 5b) assays. The LDH and MTT assays are commonly used in cell culture studies to assess cell death and cell viability, respectively. They were employed as complementary assays in our investigation of NP-induced changes to cell health in order to ensure a robust and reliable assessment that was not confounded by any inherent weaknesses of either assay. The LDH assay assesses cell death that is evidenced by leakage into the growth medium of intracellular lactate dehydrogenase as a result of treatment-induced compromise to the integrity of the cell membrane (compromised cell membrane is characteristic of early necrosis or late apoptosis). On the other hand, the MTT assay indicates treatment-induced changes to cell viability by assessing the extent of the purple formazan product formed as a result of the reduction of MTT by mitochondrial succinate dehydrogenase. It is shown in Fig. 5a that **AP-6** NPs were more toxic than **AP-3** NPs, despite both having similar zeta potential (Table 2). Fig. 5a presents that cytotoxicity of **AP-3** was amphiphilic concentration independent (from 0.0469 mg/mL to 0.75 mg/mL), while the cytotoxicity for **AP-6** NPs were amphiphilic peptide concentration dependent. This might be explained by the fact that the CMC for **AP-3** (40 mg/L) was lower than that for **AP-6** (75 mg/L) (Table 2). Therefore, the higher toxicity of **AP-6** NPs may be due to the more free-amphiphilic peptides of **AP-6** in the media with more positive charge in each construct than of **AP-3** ones, which acted like a surfactant and lysed the cells. Fig. 5a illustrates that all NPs showed cytotoxicity significantly higher than the control. However, Fig. 5b demonstrates that only **AP-3** NPs did not show cytotoxicity in the 0.0469–0.75 mg/mL concentration range. Therefore, this data indicated that **AP-3** NPs were less toxic than other NP formulations.

AP-2 and **AP-7** constructs also showed a significant increase in cell toxicity with increasing amphiphilic peptide concentration (Fig. 5a), while, **AP-9** did not show significant change in the cell toxicity by increasing the construct concentration. **AP-3** and **AP-9** showed significantly lower toxicity compared to the positive control (DMSO 5%) at all concentrations. By contrast, **AP-6** and **AP-7** showed significantly higher cytotoxicity compared to the positive control at 0.75 mg/mL construct concentration. A similar trend of cell toxicity was observed when the MTT assay was used (Fig. 5b), although in that case **AP-9** showed amphiphilic peptide concentration dependent cytotoxicity. The cytotoxicity of the NP formulations was also assessed on HeLa cells (Fig. 5c), and the cell toxicity trend was similar to what was observed in SH-SY5Y cells (Fig. 5a). Microscopic images are shown in Fig. S13 for the cell toxicity at different concentrations. **AP-8** also showed cell viability of 60.57 ± 7.13%, 41.69 ± 3.36%, and 6.08 ± 1.08% for the **AP-8** concentrations of 0.0469 mg/mL, 0.1875 mg/mL and 0.75 mg/mL, respectively, similar to **AP-7.** Therefore, **AP-1**, **AP-2**, **AP-7** and **AP-8** were not further investigated following the cytotoxicity outcomes.

Uptake of NPs by Brain Endothelial and Neuronal Cells

We evaluated the complex formation between FAM-siRNA and **AP-3** and **AP-6** using an agarose gel retardation assay. It was found

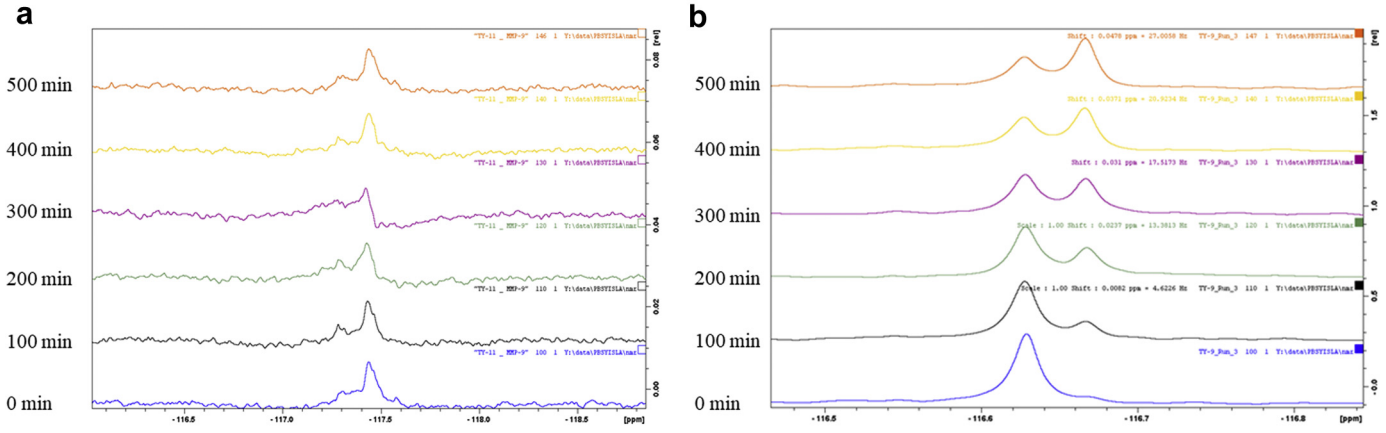

Fig. 4. Shift in the ^{19}F NMR spectra of a) NPs with the construct of C_{27}-GGGRPLGLW**CDIF**^{19}**TNSRGKRA** in the presence of active MMP-9 over time, showing a poor signal-to-noise ratio as well as no considerable change in the signal over time. b) MMP-9 responsive peptide (PLGLWG^{19}FQ) in the presence of active MMP-9 over time, presenting a high signal-to-noise ratio as well as considerable change in the signal over time.

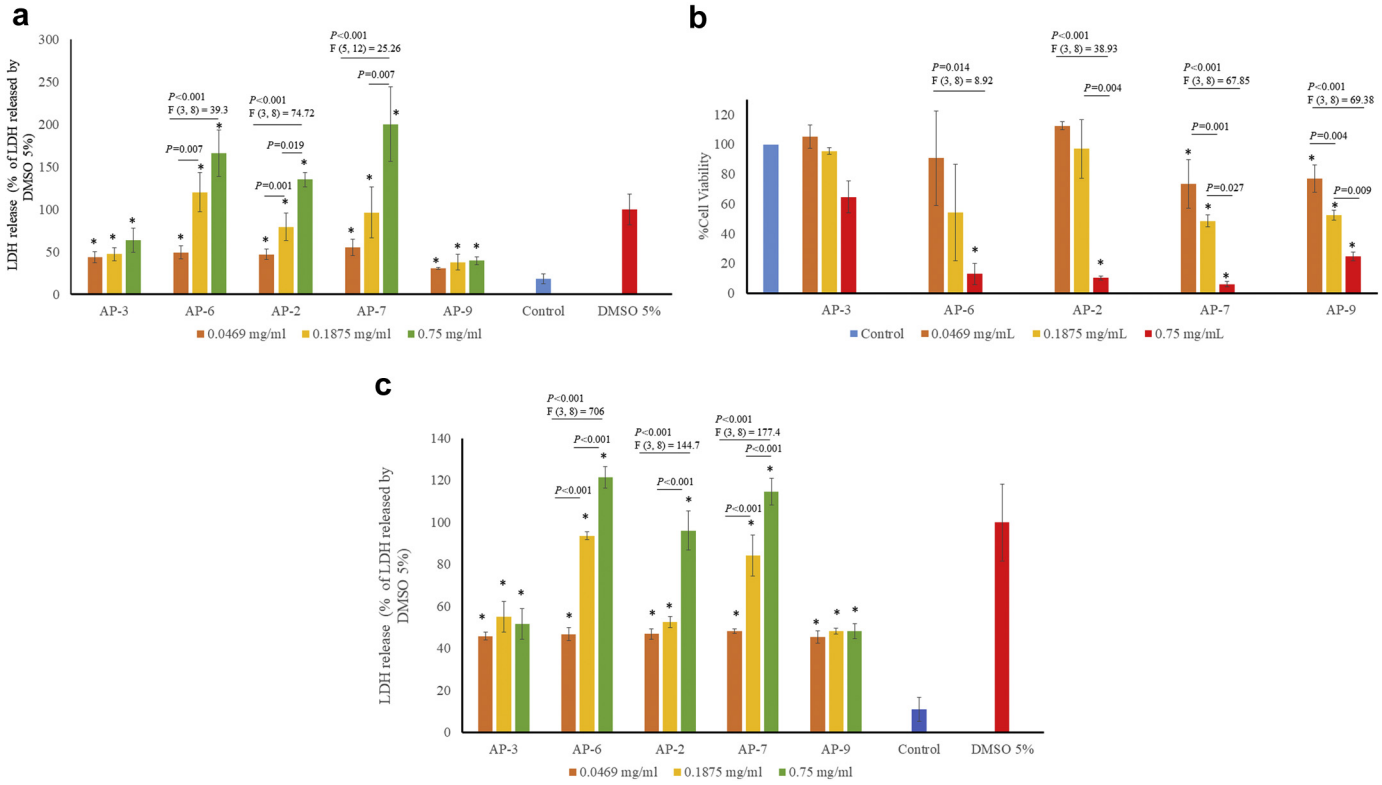

Fig. 5. Cell toxicity of **AP-3**, **AP-2**, **AP-6**, **AP-7** and **AP-9** at different concentrations (0.0469, 0.1875 and 0.75 mg/mL), assessed using the: a) LDH assay on SH-SY5Y cells, b) MTT assay on SH-SY5Y cells, c) LDH assay on HeLa cells. Significant statistical differences ($P < 0.05$) are indicated by "*". *F* values designate the *F*-test results. Horizontal lines show the pair that showed statistical differences. Error bars show standard deviation and each experiment was run three independent times (n = 3).

that the **AP-6** construct formed complex with FAM-siRNA at N (amine)/P(phosphate) ratio of 20 (Fig. 6). On the other hand, in preliminary studies, **AP-3** did not form a complex with an oligonucleotide at typical concentrations, and significantly a large quantity of the compound was required according to agarose gel retardation assay (Fig. S14). This could be due to the presence of only a single positive charge in the molecular structure of **AP-3**. Therefore, **AP-6** was a more effective nucleic acid binder than **AP-3**. However, it is shown in the following (Figs. 7-9) that **AP-3** NPs were able to transport FAM-siRNA across the cell membrane or the BBB model. It may be speculated that **AP-3** encapsulated FAM-siRNA in a similar way as liposomes, i.e. **AP-3** NPs were nanovesicles.

In vitro cellular uptake was analysed by flow cytometry for SHSY-5Y cells. Clear differences in the fluorescence were observed after 4 h for both **AP-3** and **AP-6** as shown in Fig. 7. Cellular uptake of encapsulated FAM-siRNA was significantly higher than the uptake of naked FAM-siRNA. It was noticed that penetration was time dependent. In the first hour, uptake was less, but it increased substantially at 4 h.

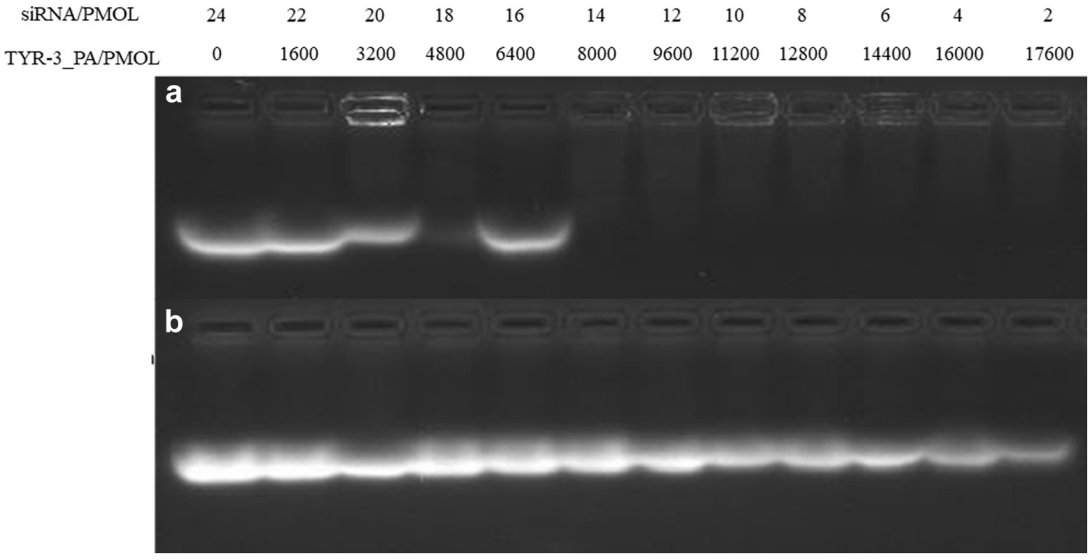

Fig. 6. Agarose gel electrophoresis of FAM-siRNA a) in complex with **AP-6** construct, b) FAM-siRNA only. Complex formed at N/P of 20.

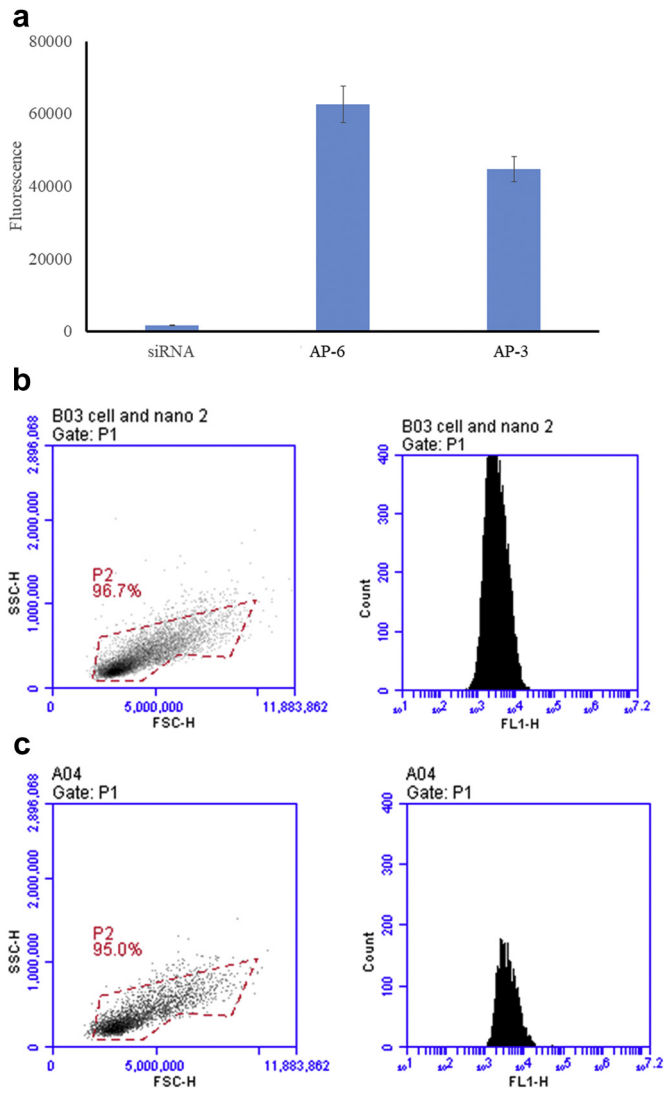

Fig. 7. *In vitro* cellular uptake of self-assembled peptide-based brain-targeting NPs. a) FACS analysis for cellular uptake (fluorescence) shown in bar chart for **AP-3**, **AP-6** and naked FAM-siRNA. b) FACS chromatogram for **AP-6** after 4 h and c) FACS chromatogram for **AP-3** after 4 h.

Cellular uptake of NPs was confirmed by confocal microscopy of brain endothelial cells (hCMEC/D3 cells). Confocal microscopy revealed that FAM-siRNA was found around the DAPI stained nucleus (Fig. 8).

NPs Crossing the In Vitro BBB Model

The fluorescence from FAM-siRNA was measured in the basolateral compartment of the BBB model; and it was found that naked FAM-siRNA penetration was around 5.78 ± 4.09% after 6 h, whereas in the presence of histamine it was around 18.7 ± 3.01% due to the disturbance of TJ caused by the histamine. Histamine followed by cimetidine treated cells showed permeability of around 5.84 ± 4.07% due to the comparative antagonism between histamine and cimetidine (Fig. 9a).[54] These experiments indicated the integrity of the BBB model against naked FAM-siRNA.

AP-6 and **AP-3** NPs showed the transmigration of 31.53 ± 2.61% and 31.03 ± 3.91% at 2 h, respectively. Then, the percentages of **AP-6** and **AP-3** NPs crossing the BBB model increased slightly to 34.54 ± 2.21% and 33.34 ± 2.36%, respectively, at 6 h as shown in Fig. 9b with P_{app} presented in Fig. 9c.

To mimic pathological conditions, active MMP-9 (140 ng/mL) was added to the basolateral compartment. The fraction of **AP-3** NPs crossing the BBB increased to 40.96 ± 5.82% at 6 h and did not change significantly up to 24 h, while the percentage of **AP-6** NPs decreased from 36.09 ± 3.25% to 27.66 ± 2.69% at 24 h (Fig. 9d with P_{app} illustrated in Fig. 9e). This may be due to the resistance of **AP-6** NPs to MMP-9, which permitted them to transmigrate back to the apical compartment.

In the next step, activated MMP-9 was added in both the apical (50 ng/mL) and basolateral (140 ng/mL) compartments. This led to a slight decrease in the permeability after 6 h for both **AP-6** and **AP-3** NPs, 34.81 + 0.73% and 33.49 ± 1.57%, respectively (Fig. 9f with P_{app} illustrated in Fig. 9g), compared to the condition with active MMP-9 only in the basolateral compartment(Fig. 9d). However, the fraction of **AP-3** NPs transmigrating the BBB increased to 70.75 ± 5.78% at 24 h, while this decreased to 29.64 ± 0.91% for **AP-6** NPs (Fig. 9f).

In the final step, activated MMP-9 was added at higher concentration to the apical compartment (100 ng/mL) but maintained at 140 ng/mL for the basolateral compartment to simulate pathological conditions, when MMP-9 levels are significantly elevated both in the blood circulation and the brain. Fig. 9h illustrates that the fraction of **AP-3** NPs transmigrating the BBB increased to 43.17 ± 6.75% at 2 h, but dropped to 25.04 ± 0.67% at 6 h. Similar to the previous case, that the percentage increased only to 51.19 ± 2.06% at 24 h. Fig. 9i presents P_{app} values for the latter case. Interestingly, **AP-9** NPs bounced between the apical and basolateral compartments during 24 h (Fig. 9g). The percentage of **AP-9** NPs transmigrated across the BBB was 52.45 ± 6.73% at 2 h, but that decreased to 16.51 ± 2.29% at 3 h, much less than the percentage for **AP-3** (37.23 ± 6.25%). These observations could be due to the fact that **AP-9** did not have a MMP-9 sensitive sequence in the construct. Hence, the NPs moved freely between both compartments, but for **AP-3** NPs, the damage from the MMP-9 led to accumulation more in one compartment compared to the other one. These show that higher active MMP-9 levels in the apical compartment reduced the final number of NPs in the basolateral compartment for **AP-3**. Only moderately active MMP-9 levels in the apical compartment (50 ng/mL) made 71% of NPs accumulating in the basolateral compartment at 24 h.

TEER values before and after the NP treatment were 239 ± 28 Ω cm^{-2} and 250 ± 13 Ω cm^{-2}, respectively for 100 ng/mL of MMP-9 in the apical chamber and 140 ng/mL in the basolateral chamber. The TEER values were high enough to reflect the BBB tightness for BBB transmigration purposes. Also, the permeability of FITC-dextran was less than 2.5% after 6 h post NP treatment (with MMP-9), confirming the passage of FAM-siRNA was due to the NPs. This data suggested the integrity of the monolayer during the tests.

Haemolysis and Cytokine Release by NPs

Fig. 10a presents the haemolysis results of **AP-3** for the blood sample of three volunteers. It can be seen that **AP-3** did not cause more than 5% haemolysis in the concentration range of 50–500 μg/mL; except for Donor 1, in which haemolysis was just above 5%. On the other hand, the haemolysis of **AP-6** (Fig. 10b) was significantly greater than 5% for both 250 μg/mL and 500 μg/mL for all three donors. The **AP-6** haemolysis decreased to 5% at 100 μg/mL for Donor 3, while those were greater than 5% for both Donor 1 and Donor 2. The haemolysis of **AP-6** was about 5% at 50 μg/mL for all donors. These observations show that different human subjects may elicit significantly different haemolysis on exposure to NPs. It

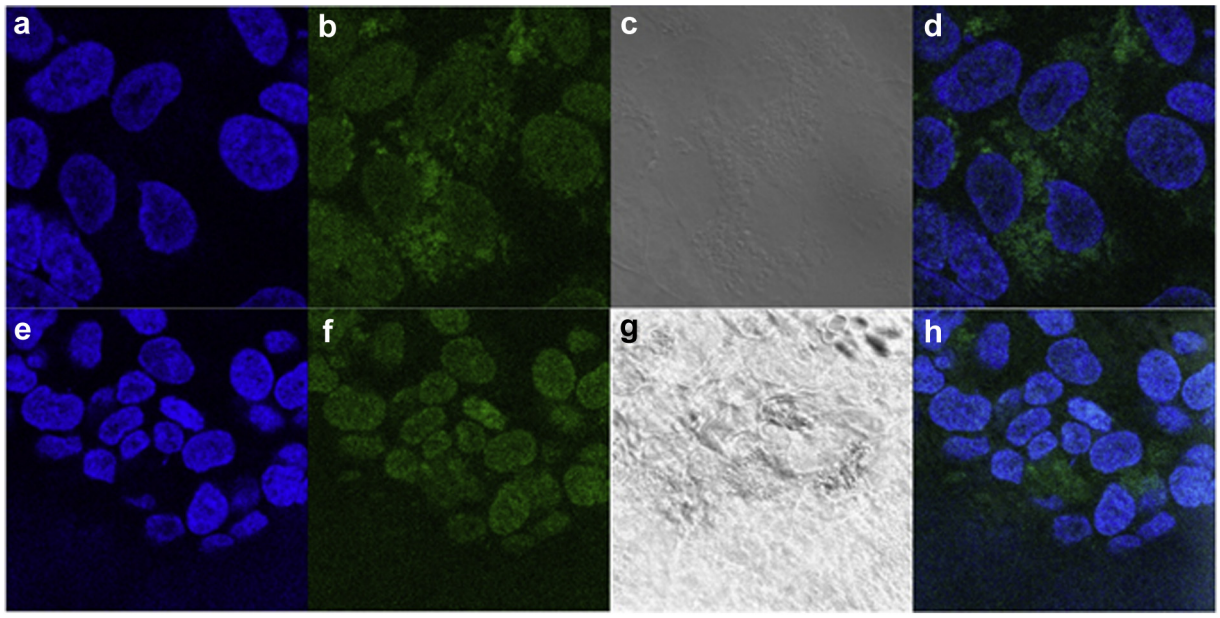

Fig. 8. Confocal images of self-assembled enzyme responsive peptide-based brain-targeting NPs: **AP-6** (a-d) and **AP-3** (e-f) in the hCMEC/D3 cell line after 24 h treatment. Confocal images showing the localisation of NPs around the nucleus. a and e are DAPI stained nucleus, b and f are NPs (FAM channel), c and g are bright field images of cells, d and h are overlaid images.

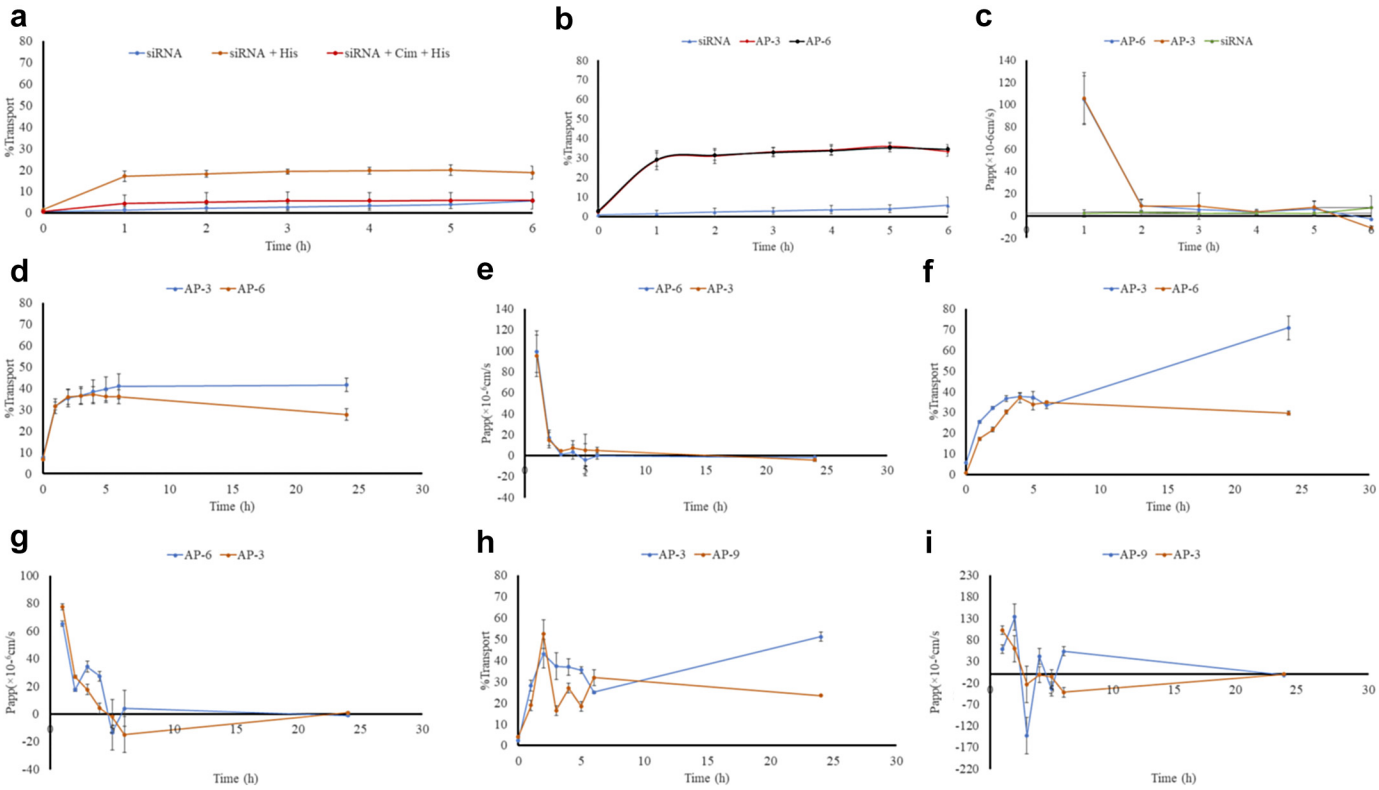

Fig. 9. *In vitro* BBB transmigration and permeability of novel enzyme-responsive self-assembled peptide-based brain-targeting NPs in the hCMEC/D3 cell line. a) BBB transmigration of naked FAM-siRNA alone, in the presence of histamine, and cimetidine, showing transmigration of naked FAM-siRNA through the BBB when the BBB permeability was increased by the addition of histamine, but FAM-siRNA transmigration through the BBB was decreased when cimetidine was added due to the recovery of the tight junctions. b) BBB transmigration of naked FAM-siRNA, **AP-6** and **AP-3**, showing transmigration of FAM-siRNA by the **AP-6** and **AP-3** NPs. c) The permeability presentation of data in panel B. d) BBB transmigration of **AP-3** and **AP-6** in the presence of active MMP-9 (140 ng/mL) in the basolateral compartment, indicating slight decrease in the percentage of **AP-6** NPs in the basolateral compartment due to the backflow of the NPs to the apical compartment. e) Permeability calculations of data in panel D. f) BBB transmigration of **AP-3** and **AP-6** NPs in the presence of active MMP-9 in both the apical (50 ng/mL) and basolateral (140 ng/mL) compartments with **AP-3** NPs reaching 70.75 ± 5.78% transmigration at 24 h due to the damaged imposed by the MMP-9 to the NPs at the basolateral compartment. g) The permeability presentation of data in panel F. h) BBB transmigration of **AP-3** and **AP-9** in the presence of active MMP-9 in both the apical (100 ng/mL) and basolateral (140 ng/mL) compartments, presenting back and forth flow of **AP-9** NPs between the apical and basolateral compartments with a lesser extent for AP-3 NPs. i) The permeability presentation of data in panel H. Error bars show standard deviation and each experiment was run three independent times (n = 3).

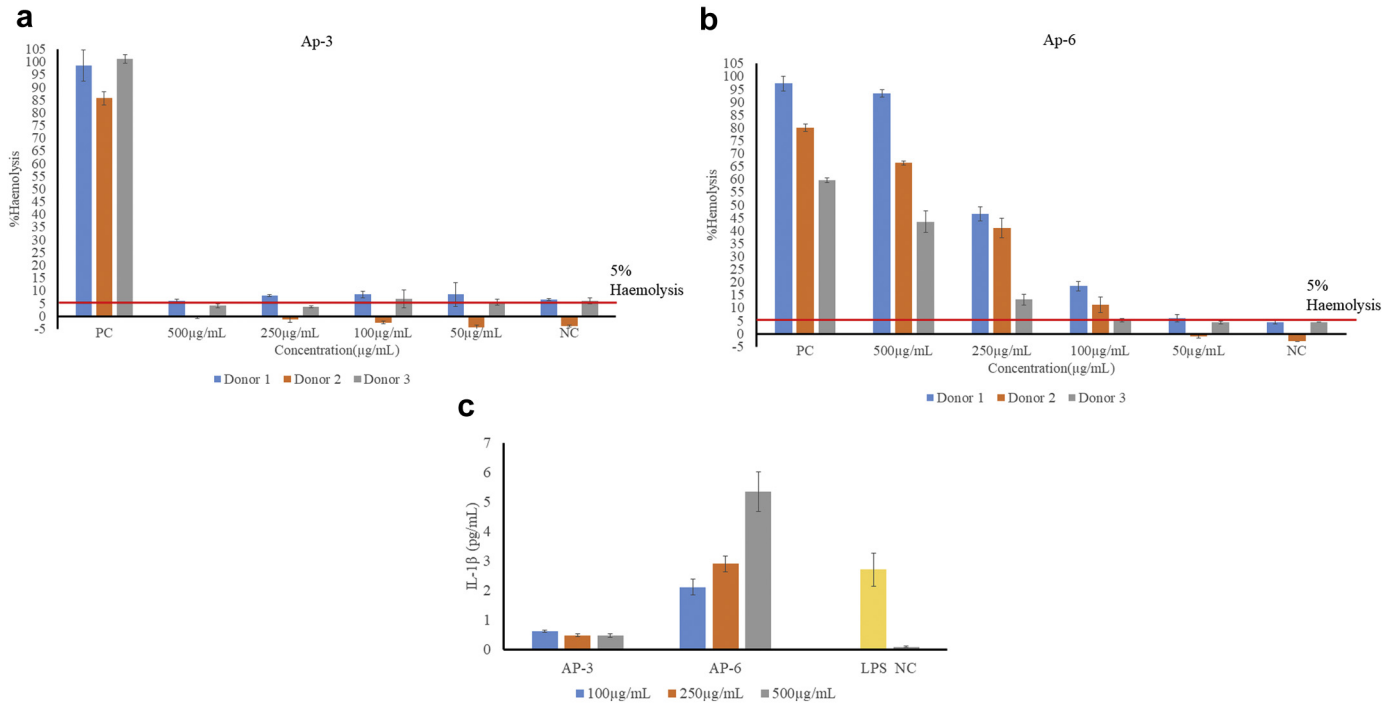

Fig. 10. Blood compatibility of MMP-9 responsive peptide-based brain-targeting NPs. a) haemolysis of **AP-3.** b) haemolysis of **AP-6**, showing significant haemolysis by **AP-6** NPs compared to **AP-3** NPs. c) IL-1β release from THP-1 cells in the presence of **AP-3** and **AP-6**, illustrating significant cytokine release by **AP-6** NPs compared to **AP-3** NPs. Error bars show standard deviation and each experiment was run three independent times (n = 3).

may be argued that those NPs will be acceptable that do not exert more than 5% haemolysis for most subjects, if not all.

Fig. 10c illustrates the release of cytokine IL-1β from THP-1 cells in the presence of **AP-3** and **AP-6** NPs. It can be seen that **AP-3** NPs caused the release of more IL-1β cytokine than the negative control (NC), but the quantities were less than 1 pg/mL at all construct concentrations (100−500 µg/mL). On the other hand, **AP-6** NPs triggered the release of 2.12 ± 0.27 pg/mL of IL-1β cytokine at 100 µg/mL; and the release increased to 2.91 ± 0.26 pg/mL and 5.36 ± 0.66 pg/mL at 250 µg/mL and 500 µg/mL **AP-6** concentrations, respectively. Fig. 10c also shows that the amounts of IL-1β released from THP-1 cells in the presence of **AP-6** NPs at 500 µg/mL concentration was even greater than the positive control.

Discussion

In this study, we compared different MMP-9 responsive self-assembled brain-targeting peptide-based NPs that can cross the BBB. These NPs were also able to penetrate the neural cells because of the inclusion of a brain targeting ligand.[24,25] The NPs showed positive zeta potential values, which is a desirable property since it will further facilitate the binding of the particles to the negatively charged lipid bilayer membrane of the BBB.[37] The CMCs for all the formulations were closer to the previously reported CMC of an amphiphilic brain-targeting peptide (36.1 mg/L)[37] except for **AP-5**. The particle size measurements by the DLS and TEM or SEM were different. The reason could be due to the fact that DLS measures hydrodynamic particle size,[55] whereas in TEM particle size is measured individually without interaction with solvent molecules,[56] or other NPs.[57] In addition, DLS can identify larger particles more easily compared to smaller particles.[58]

The encapsulation efficiency of FSS for **AP-6** and **AP-3** were 77.85 ± 4.16% and 79.60 ± 3.36% respectively, which are close to loading capacity of previously reported peptide-based NPs.[59] Surprisingly, the release of FSS was not higher than distilled water in the presence of active MMP-9 for **AP**s with MMP-9 cleavable peptide. This was partly due to the retardation effects of TNCB buffer components (the enzyme buffer) on the FSS release; and NMR data suggested the burial of MMP-9 cleavable sequence within the core of the NPs. This interpretation was based on the use of ^{19}F NMR to study the aggregation of $A\beta_{1-40}$, and the intensity of the NMR signal reduced due to the aggregation of ^{19}F labelled $A\beta_{1-40}$.[60] Therefore, reduced intensity of ^{19}F NMR signal of NPs in our study compared to a ^{19}F labelled peptide suggested hiding of ^{19}F labelled parts of the amphiphilic peptides within the NP's core. Within the NPs, **AP-3** showed the highest responsiveness to MMP-9. Perhaps this was due to the brain-targeting ligand being responsive to MMP-9 and these peptides were accessible to active MMP-9 enzyme.

In the presence of BSA, release of FSS decreased significantly. One of the possible explanations could be the formation of a protein corona that prevents the release of encapsulated drugs.[61] Our data showed an increase in the size of NPs in the presence of BSA, while brain-targeting solid lipid NPs did not show any changes in size in the presence of human serum.[62]

In vitro permeability was assessed using hCMEC/D3 BBB model, which has also been investigated by other researchers.[63–65] **AP-3** NPs achieved up to 71% of total NPs crossing the BBB model in the presence of active MMP-9, indicating that NPs could achieve a high efficiency in crossing the BBB in the presence of active MMP-9 when the brain-targeting motif is responsive to MMP-9, which mediated cleavage. The encouraging results of this *in vitro* study now pave the way for an *in vivo* experiment to explore the potential of our novel NPs in delivering therapeutic agents to the brain.[66] Furthermore, the *in vivo* work will identify the body distribution of the NPs (off-targets) and potential side effects. However, the results of this work indicated degradation of the NPs by serum enzymes within 24 h.

It should be noted that enzyme-responsive NPs have been developed for the treatment of brain diseases.[67–69] In one approach, the core of the NPs contained a peptide crosslinker that was cleavable by MMP-2. Initially, the monomer (2-methacryloyloxyethyl phosphorylcholine) and crosslinker were augmented around individual monoclonal antibodies (mAbs); which followed by polymerization to grow a thin shell of polymer around the mAb molecules, forming the nanocapsules of mAbs.[67] In another approach, the NPs contained a core composed of gelatine, which is degradable by MMP-2. The surface of the gelatine NPs was conjugated with gold NPs carrying doxorubicin and RRGD (a glioma targeting peptide) (G-AuNPs-DC-RRGD).[69] The NPs originally had a size of 188 nm, but in the presence of MMP-2, they shrank to 55 nm, allowing improved diffusion into the brain parenchyma. Intravenous injection of G-AuNPs-DC-RRGD NPs led to the accumulation of the NPs in the glioma of C6 cell xenograft-bearing mice 4 h post injection.[67] Finally, block copolymers were produced containing either NH_2-norleucineTPRSFL-C-SH, a thrombin-cleavable peptide (T), or NH_2-LGRMGLPGK-C-SH (M), a MMP-9-cleavable peptide.[68] The block copolymers were obtained by conjugating the PEGylated peptides to poly(ε-caprolactone) monomers. PEG-T-poly(ε-caprolactone) or PEG-*M*-poly(ε-caprolactone) monomers were used to form nanocarriers by precipitation, and these were cleavable by thrombin, or MMP-9, respectively.[68] The PEG-T-poly(ε-caprolactone) NPs expanded from sub 100 nm size to over 1000 nm size after 24 h incubation with thrombin. Similar observation was made for PEG-*M*-poly(ε-caprolactone) NPs in the presence of MMP-9. The aim of the expanding nanocarriers was to prevent return of nanocarriers from the abluminal side of the BBB to the luminal side by transcytosis.[68] These approaches are efficient methods in delivering of therapeutic agents to the brain, and the advantage of our **AP**s is the formation of NPs instantly, potentially in the clinic for the purpose of personalised medicine for the treatment of brain diseases.

AP-3 NPs caused the release of much lower amounts of IL-1β than LPS treated cells, but slightly higher than negative control, a trend similar to another type of peptide-based brain-targeting NPs.[70] Cytokine release is affected by concentration[71–73] and charge[74] of NPs. **AP-6** presented increase in the release of IL-1β in a clear concentration-dependent trend. Although **AP-3** and **AP-6** NPs carried similar zeta potential, the higher construct charge of **AP-6** (3+) could be part of the higher cytokine release compared to the lower construct charge of **AP-3** (1+). Furthermore, as the cytotoxicity of **AP-6** was greater than **AP-3**, then the lysis of cells would potentially explain why THP-1 cells become proinflammatory in the presence of **AP-6**, i.e. the remaining cells recognise the damage-associated molecular patterns that are released by lysed cells. The release of cytokines is a biomarker of immunotoxicity which may lead to fever or life-threatening reactions.[75]

AP-3 NPs showed less than 5% haemolysis at all concentrations, while **AP-6** showed more than 5% haemolysis at concentrations above 100 μg/mL. A previous work also showed significant haemolysis for cholesterol-TAT (Cholestrol-YGRKKRRQRRR) amphiphilic peptide-based brain-targeting NPs.[37] In addition, amphiphilic peptides (C_{16}-W-I-L-A2-G3-K9-TAT) showed haemolysis at lower concentrations such as 25 μg/mL.[76] Comparing the construct of **AP-6**, cholesterol-TAT and C_{16}-W-I-L-A2-G3-K9-TAT NPs reveals that the increased haemolysis for these **AP**s could be due to the high number of positive charges on the amphiphilic molecule. Interestingly, PAMAM G4 dendrimer (G4) induced less than 5% haemolysis at concentrations as high as 1280 μg/mL, in which the constructs contained 64 primary amine groups.[77] These observations suggest that carrying positive charge may not be the only cause of haemolysis, and the presence of a hydrophobic moiety in the construct is essential. When brain-targeting NPs are administered intravenously, these should not cause haemolysis as loss of red blood cells may lead to anaemia.

Electrophoresis, cellular uptake and BBB transmigration studies suggested nanovesicle structure for **AP-3** construct. Previous studies have also found formation of nanovesicles by amphiphilic peptides.[78–81]

Conclusion

In this work, we identified a simple amphiphilic peptide construct, cholesterol-GGGCKAPETALC, which self-assembled to NPs with the size of 80 nm and had no significant toxicity up to 0.75 mg/mL. The NPs encapsulated FAM-siRNA and transmigrated across an *in vitro* BBB model. These NPs showed minimal haemolysis and IL-1β cytokine release. The data suggested that these NPs would transport more therapeutic agent across the BBB when the active MMP-9 levels are elevated in both the blood stream and brain interstitial fluid. The presence of MMP-9 cleavable peptide did not increase the permeability of NPs crossing the BBB. Most likely, MMP-9 damaged the NPs through the MMP-9 cleavable sequence and prevented the return of the NPs from the basolateral compartment to the apical compartment.

Conflicts of interest

The authors declare no conflict of interest.

Acknowledgement

We would like to thank technical assistance of Gabriela Rudnicka and Jack Lonergan. Also, we are grateful for the support of the EU's Erasmus + programme.

Appendix A. Supplementary data

Supplementary data to this article can be found online at https://doi.org/10.1016/j.xphs.2020.12.004.

References

1. Amor S, Puentes F, Baker D, van der Valk P. Inflammation in neurodegenerative diseases. *Immunology*. 2010;129(2):154-169.
2. Heemels M-T. Neurodegenerative diseases. *Nature*. 2016;539:179.
3. Gitler AD, Dhillon P, Shorter J. Neurodegenerative disease: models, mechanisms, and a new hope. *Dis Model Mech*. 2017;10(5):499-502.
4. Josephs KA, Ahlskog JE, Parisi JE, et al. Rapidly progressive neurodegenerative dementias. *Arch Neurol*. 2009;66(2):201-207.
5. Gan L, Cookson MR, Petrucelli L, La Spada AR. Converging pathways in neurodegeneration, from genetics to mechanisms. *Nat Neurosci*. 2018;21(10):1300-1309.
6. Prince M, Knapp M, Guerchet M, et al. *Dementia UK: -overview*. 2014.
7. Pan S, Huang X, Wang Y, et al. Efficacy of intravenous plus intrathecal/intracerebral ventricle injection of polymyxin B for post-neurosurgical intracranial infections due to MDR/XDR Acinectobacter baumannii: a retrospective cohort study. *Antimicrob Resist Infect Contr*. 2018;7(1):8.
8. Kim J-Y, Grunke SD, Levites Y, Golde TE, Jankowsky JL. Intracerebroventricular viral injection of the neonatal mouse brain for persistent and widespread neuronal transduction. *JoVE*. 2014;91:51863.
9. Rodriguez M, Lapierre J, Ojha CR, et al. Intranasal drug delivery of small interfering RNA targeting Beclin1 encapsulated with polyethylenimine (PEI) in mouse brain to achieve HIV attenuation. *Sci Rep*. 2017;7(1):1862.
10. Oller-Salvia B, Sánchez-Navarro M, Giralt E, Teixidó M. Blood-brain barrier shuttle peptides: an emerging paradigm for brain delivery. *Chem Soc Rev*. 2016;45(17):4690-4707.
11. Gonzalez-Carter DA, Ong ZY, McGilvery CM, Dunlop IE, Dexter DT, Porter AE. L-DOPA functionalized, multi-branched gold nanoparticles as brain-targeted nano-vehicles. *Nanomed Nanotechnol Biol Med*. 2019;15(1):1-11.
12. Lakkadwala S, Singh J. Co-delivery of doxorubicin and erlotinib through liposomal nanoparticles for glioblastoma tumor regression using an in vitro brain tumor model. *Colloids Surf B Biointerf*. 2019;173:27-35.

13. Rassu G, Porcu E, Fancello S, et al. Intranasal delivery of genistein-loaded nanoparticles as a potential preventive system against neurodegenerative disorders. *Pharmaceutics*. 2018;11(1):8.
14. Yuan B, Zhao Y, Dong S, et al. Cell-penetrating peptide-coated liposomes for drug delivery across the blood−brain barrier. *Anticancer Res*. 2019;39(1):237-243.
15. Ammar HO, Ghorab MM, Mahmoud AA, Higazy IM. Lamotrigine loaded poly-ϵ-(d,l-lactide-co-caprolactone) nanoparticles as brain delivery system. *Eur J Pharmaceut Sci*. 2018;115:77-87.
16. Miao Y-F, Peng T, Moody MR, et al. Delivery of xenon-containing echogenic liposomes inhibits early brain injury following subarachnoid hemorrhage. *Sci Rep*. 2018;8(1):450.
17. Kojima R, Bojar D, Rizzi G, et al. Designer exosomes produced by implanted cells intracerebrally deliver therapeutic cargo for Parkinson's disease treatment. *Nat Commun*. 2018;9(1):1305.
18. Moscariello P, Ng DYW, Jansen M, Weil T, Luhmann HJ, Hedrich J brain delivery of multifunctional dendrimer protein bioconjugates. Adv Sci 0(0):1700897.
19. Ghorbani M, Bigdeli B, Jalili-baleh L, et al. Curcumin-lipoic acid conjugate as a promising anticancer agent on the surface of gold-iron oxide nanocomposites: a pH-sensitive targeted drug delivery system for brain cancer theranostics. *Eur J Pharmaceut Sci*. 2018;114:175-188.
20. Díaz-Perlas C, Oller-Salvia B, Sánchez-Navarro M, Teixidó M, Giralt E. Branched BBB-shuttle peptides: chemoselective modification of proteins to enhance blood−brain barrier transport. *Chem Sci*. 2018;9(44):8409-8415.
21. Wang D, El-Amouri SS, Dai M, et al. Engineering a lysosomal enzyme with a derivative of receptor-binding domain of apoE enables delivery across the blood-brain barrier. *Proc Natl Acad Sci U S A*. 2013;110(8):2999-3004.
22. Böckenhoff A, Cramer S, Wölte P, et al. Comparison of five peptide vectors for improved brain delivery of the lysosomal enzyme arylsulfatase A. *J Neurosci*. 2014;34(9):3122.
23. Kumar P, Wu H, McBride JL, et al. Transvascular delivery of small interfering RNA to the central nervous system. *Nature*. 2007;448(7149):39-43.
24. Javed H, Menon SA, Al-Mansoori KM, et al. Development of nonviral vectors targeting the brain as a therapeutic approach for Parkinson's disease and other brain disorders. *Mol Ther*. 2016;24(4):746-758.
25. Oller-Salvia B, Sanchez-Navarro M, Ciudad S, et al. MiniAp-4: a venom-inspired peptidomimetic for brain delivery. *Angew Chem*. 2016;55(2):572-575.
26. Muldoon LL, Pagel MA, Kroll RA, Roman-Goldstein S, Jones RS, Neuwelt EA. A physiological barrier distal to the anatomic blood-brain barrier in a model of transvascular delivery. *AJNR Am J Neuroradiol*. 1999;20(2):217-222.
27. Somogyi G, Buchwald P, Nomi D, Prokai L, Bodor N. Targeted drug delivery to the brain via phosphonate derivatives II. Anionic chemical delivery system for zidovudine (AZT). *Int J Pharm*. 1998;166(1):27-35.
28. Hadass O, Tomlinson BN, Gooyit M, Chen S, Purdy JJ, Walker JM, Zhang C, Giritharan AB, Purnell W, Robinson CR, , II, Shin D, Schroeder VA, Suckow MA, Simonyi A, Sun G Y, Mobashery S, Cui J, Chang M, Gu Z. Selective inhibition of matrix metalloproteinase-9 attenuates secondary damage resulting from severe traumatic brain injury. *PLoS One*. 2013;8(10):e76904.
29. Brkic M, Balusu S, Libert C, Vandenbroucke RE. Friends or foes: matrix metalloproteinases and their multifaceted roles in neurodegenerative diseases. *Mediat Inflamm*. 2015;2015:620581.
30. Thiele NA, Kärkkäinen J, Sloan KB, Rautio J, Huttunen KM. Secondary carbamate linker can facilitate the sustained release of dopamine from brain-targeted prodrug. *Bioorg Med Chem Lett*. 2018;28(17):2856-2860.
31. Grzybowski BA, Wilmer CE, Kim J, Browne KP, Bishop KJ. Self-assembly: from crystals to cells. *Soft Matter*. 2009;5(6):1110-1128.
32. Grzelczak M, Vermant J, Furst EM, Liz-Marzán LM. Directed self-assembly of nanoparticles. *ACS Nano*. 2010;4(7):3591-3605.
33. Ghosh R, Tabrizi SJ. Gene suppression approaches to neurodegeneration. *Alzheimers Res Ther*. 2017;9(1):82.
34. Datta G, Chaddha M, Garber DW, et al. The receptor binding domain of apolipoprotein E, linked to a model class A amphipathic helix, enhances internalization and degradation of LDL by fibroblasts. *Biochemistry*. 2000;39(1):213-220.
35. Böckenhoff A, Cramer S, Wölte P, et al. Comparison of five peptide vectors for improved brain delivery of the lysosomal enzyme arylsulfatase A. *J Neurosci*. 2014;34(9):3122-3129.
36. Ramesh S, de la Torre BG, Albericio F, Kruger HG, Govender T. Microwave-assisted synthesis of antimicrobial peptides. In: Hansen PR, ed. *Antimicrobial Peptides: Methods and Protocols*. New York, NY: Springer New York; 2017:51-59.
37. Liu L, Xu K, Wang H, et al. Self-assembled cationic peptide nanoparticles as an efficient antimicrobial agent. *Nat Nanotechnol*. 2009;4:457.
38. Li C-G, Tang W, Chi X-J, Dong Z-M, Wang X-X, Wang X-J. A cholesterol Tag at the N terminus of the relatively broad-spectrum fusion inhibitory peptide targets an earlier stage of fusion glycoprotein activation and increases the peptide's antiviral potency In vivo. *J Virol*. 2013;87(16):9223-9232.
39. Nasiru T, Avila L, Levine M. Determination of critical micelle concentrations using UV-visible spectroscopy. *J High School Res*. 2011;2:1-5.
40. Mohr A, Talbiersky P, Korth HG, et al. A new pyrene-based fluorescent probe for the determination of critical micelle concentrations. *J Phys Chem B*. 2007;111(45):12985-12992.
41. Amini Y, Amel Jamehdar S, Sadri K, Zare S, Musavi D, Tafaghodi M. Different methods to determine the encapsulation efficiency of protein in PLGA nanoparticles. *Bio Med Mater Eng*. 2017;28:613-620.
42. Islam Y, Khalid A, Pluchino S, et al. Development of brain targeting peptide based MMP-9 inhibiting nanoparticles for the treatment of brain diseases with elevated MMP-9 activity. *J Pharmaceut Sci*. 2020;109(10):3134-3144.
43. Pulford B, Reim N, Bell A, et al. Liposome-siRNA-peptide complexes cross the blood-brain barrier and significantly decrease PrP on neuronal cells and PrP in infected cell cultures. *PLoS One*. 2010;5(6):e11085.
44. Gao Y, Wang ZY, Zhang J, et al. RVG-peptide-linked trimethylated chitosan for delivery of siRNA to the brain. *Biomacromolecules*. 2014;15(3):1010-1018.
45. Yushchenko M, Weber F, Mäder M, et al. Matrix metalloproteinase-9 (MMP-9) in human cerebrospinal fluid (CSF): elevated levels are primarily related to CSF cell count. *J Neuroimmunol*. 2000;110(1-2):244-251.
46. Takeshita S, Tokutomi T, Kawase H, et al. Elevated serum levels of matrix metalloproteinase-9 (MMP-9) in Kawasaki disease. *Clin Exp Immunol*. 2001;125(2):340-344.
47. Heymans M, Sevin E, Gosselet F, Lundquist S, Culot M. Mimicking brain tissue binding in an in vitro model of the blood-brain barrier illustrates differences between in vitro and in vivo methods for assessing the rate of brain penetration. *Eur J Pharm Biopharm*. 2018;127:453-461.
48. Neun BW, Ilinskaya AN, Dobrovolskaia MA. Updated method for in vitro analysis of nanoparticle hemolytic properties. In: McNeil SE, ed. *Characterization of Nanoparticles Intended for Drug Delivery*. New York, NY: Springer New York; 2018:91-102.
49. Liptrott NJ, Giardiello M, McDonald TO, Rannard SP, Owen A. Assessment of interactions of efavirenz solid drug nanoparticles with human immunological and haematological systems. *J Nanobiotechnol*. 2018;16(1):22.
50. Huang H, Lai W, Cui M, et al. An evaluation of blood compatibility of silver nanoparticles. *Sci Rep*. 2016;6(1):25518.
51. Daigneault M, Preston JA, Marriott HM, Whyte MK, Dockrell DH. The identification of markers of macrophage differentiation in PMA-stimulated THP-1 cells and monocyte-derived macrophages. *PLoS One*. 2010;5(1):e8668.
52. Potter TM, Neun BW, Rodriguez JC, Ilinskaya AN, Dobrovolskaia MA. Analysis of pro-inflammatory cytokine and type II interferon induction by nanoparticles. *Methods Mol Biol*. 2018;1682:173-187.
53. Lamort AS, Gravier R, Laffitte A, Juliano L, Zani ML, Moreau T. New insights into the substrate specificity of macrophage elastase MMP-12. *Biol Chem*. 2016;397(5):469-484.
54. Wang Z, Cai X-J, Qin J, Xie F-J, Han N, Lu H-Y. The role of histamine in opening blood-tumor barrier. *Oncotarget*. 2016;7(21):31299-31310.
55. Lim J, Yeap SP, Che HX, Low SC. Characterization of magnetic nanoparticle by dynamic light scattering. *Nanoscale Res Lett*. 2013;8(1):381.
56. Domingos RF, Baalousha MA, Ju-Nam Y, et al. Characterizing manufactured nanoparticles in the environment: multimethod determination of particle sizes. *Environ Sci Technol*. 2009;43(19):7277-7284.
57. Souza TGF, Ciminelli VST, Mohallem NDS. A comparison of TEM and DLS methods to characterize size distribution of ceramic nanoparticles. *J Phys Conf*. 2016;733:12039.
58. Fissan H, Ristig S, Kaminski H, Asbach C, Epple M. Comparison of different characterization methods for nanoparticle dispersions before and after aerosolization. *Anal Methods*. 2014;6(18):7324-7334.
59. Pandit G, Roy K, Agarwal U, Chatterjee S. Self-assembly mechanism of a peptide-based drug delivery vehicle. *ACS Omega*. 2018;3(3):3143-3155.
60. Suzuki Y, Brender JR, Soper MT, et al. Resolution of oligomeric species during the aggregation of Aβ1-40 using (19)F NMR. *Biochemistry*. 2013;52(11):1903-1912.
61. Su G, Jiang H, Xu B, Yu Y, Chen X. Effects of protein corona on active and passive targeting of cyclic RGD peptide-functionalized PEGylation nanoparticles. *Mol Pharm*. 2018;15(11):5019-5030.
62. Arduino I, Depalo N, Re F, et al. PEGylated solid lipid nanoparticles for brain delivery of lipophilic kiteplatin Pt(IV) prodrugs: an in vitro study. *Int J Pharm*. 2020;583:119351.
63. Tega Y, Tabata H, Kurosawa T, et al. Structural requirements for uptake of diphenhydramine analogs into hCMEC/D3 cells via the proton-coupled organic cation antiporter. *J Pharmaceut Sci*. 2020;110(1):397-403.
64. Lopalco A, Ali H, Denora N, Rytting E. Oxcarbazepine-loaded polymeric nanoparticles: development and permeability studies across in vitro models of the blood-brain barrier and human placental trophoblast. *Int J Nanomed*. 2015;10:1985-1996.
65. Wu LP, Ahmadvand D, Su J, et al. Crossing the blood-brain-barrier with nanoligand drug carriers self-assembled from a phage display peptide. *Nat Commun*. 2019;10(1):4635.
66. Somani S, Robb G, Pickard BS, Dufès C. Enhanced gene expression in the brain following intravenous administration of lactoferrin-bearing polypropylenimine dendriplex. *J Contr Release*. 2015;217:235-242.
67. Han L, Liu C, Qi H, et al. Systemic delivery of monoclonal antibodies to the central nervous system for brain tumor therapy. *Adv Mater*. 2019;31(19):e1805697.
68. Guo X, Deng G, Liu J, et al. Thrombin-responsive, brain-targeting nanoparticles for improved stroke therapy. *ACS Nano*. 2018;12(8):8723-8732.
69. Ruan S, He Q, Gao H. Matrix metalloproteinase triggered size-shrinkable gelatin-gold fabricated nanoparticles for tumor microenvironment sensitive penetration and diagnosis of glioma. *Nanoscale*. 2015;7(21):9487-9496.
70. Wu L-P, Ahmadvand D, Su J, et al. Crossing the blood-brain-barrier with nanoligand drug carriers self-assembled from a phage display peptide. *Nat Commun*. 2019;10(1):4635.

71. Li Y, Italiani P, Casals E, et al. Assessing the immunosafety of engineered nanoparticles with a novel in vitro model based on human primary monocytes. *ACS Appl Mater Interfaces*. 2016;8(42):28437-28447.
72. Cai X, Dong J, Liu J, et al. Multi-hierarchical profiling the structure-activity relationships of engineered nanomaterials at nano-bio interfaces. *Nat Commun*. 2018;9(1):4416.
73. Gurunathan S, Jeyaraj M, Kang M-H, Kim J-H. The effects of apigenin-biosynthesized ultra-small platinum nanoparticles on the human monocytic THP-1 cell line. *Cells*. 2019;8(5):444.
74. Kim JH, Kim CS, Ignacio RM, et al. Immunotoxicity of silicon dioxide nanoparticles with different sizes and electrostatic charge. *Int J Nanomed*. 2014;9(Suppl 2):183-193.
75. Elsabahy M, Wooley KL. Cytokines as biomarkers of nanoparticle immunotoxicity. *Chem Soc Rev*. 2013;42(12):5552-5576.
76. He B, Ma S, Peng G, He D. TAT-modified self-assembled cationic peptide nanoparticles as an efficient antibacterial agent. *Nanomedicine*. 2018;14(2):365-372.
77. Santos SD, Xavier M, Leite DM, et al. PAMAM dendrimers: blood-brain barrier transport and neuronal uptake after focal brain ischemia. *J Control Rel*. 2018;291:65-79.
78. Fatouros DG, Lamprou DA, Urquhart AJ, et al. Lipid-like self-assembling peptide nanovesicles for drug delivery. *ACS Appl Mater Interfaces*. 2014;6(11):8184-8189.
79. Holowka EP, Pochan DJ, Deming TJ. Charged polypeptide vesicles with controllable diameter. *J Am Chem Soc*. 2005;127(35):12423-12428.
80. Gudlur S, Sukthankar P, Gao J, et al. Peptide nanovesicles formed by the self-assembly of branched amphiphilic peptides. *PLoS One*. 2012;7(9):e45374.
81. van Hell AJ, Crommelin DJ, Hennink WE, Mastrobattista E. Stabilization of peptide vesicles by introducing inter-peptide disulfide bonds. *Pharmaceut Res*. 2009;26(9):2186-2193.